INTERFEROMETRIC CHARACTERIZATION OF WIDEBAND INCOHERENT LIGHT FROM AN ERBIUM DOPED FIBER

A Thesis

Submitted to the Faculty

of

Purdue University

by

Gregg G. Anders

In Partial Fulfillment of the

Requirements for the Degree

of

Master of Science in Electrical Engineering

May 1995

ACKNOWLEDGMENTS

I would like to thank Noni and my parents for their constant support and encouragement. I would like to thank Professor Andrew Weiner for allowing me the chance to work with him and guiding me through the course of my research.

I would also like to thank Bellcore for supplying the Erbium Doped fiber used in this research.

TABLE OF CONTENTS

LIST OF FIGURES

ABSTRACT

Anders, Gregg G. M.S.E.E., Purdue University, May 1995. Interferometric Characterization of Wideband Incoherent Light From an Erbium Doped Fiber. Major Professor: Andrew M. Weiner.

Optically pumping an erbium doped fiber will induce gain along the length of the fiber. As pump photons are absorbed, the electrons are excited to a higher energy state causing gain. In the process, some of the electrons in the excited state spontaneously relax back to the ground state and emit light. This light is called Amplified Spontaneous Emission (ASE) because it is then amplified as it propagates through the fiber. Keeping the pump power below lasing threshold, the point where gain equals loss through the fiber will result in an emission of broad band white light. This ASE is centered at 1540 nm and has a spectral width of about 30 nm.

A Mach Zehnder interferometer is used to record the interference pattern of this light as a function of the path difference between the two arms. Fourier transforming this correlation trace will produce information about the source light.

To determine whether the system accurately performs the correlation of the light in the two arms, the spectrum obtained from the Fourier transform of the fringe pattern is compared to that directly measured on an optical spectrum analyzer.

Placing a sample in one arm of the interferometer will invoke a change in the correlation pattern recorded. Three samples were used, a thick glass slide, a thin glass slide, and a silicon wafer and the changes caused by these samples is discussed.

1. INTRODUCTION

Ultrafast optical pulses are very sensitive to the optics they interact with. As the pulse duration becomes shorter and shorter, the distorting effects such as wavelength dependent dispersion increases. Using compression techniques, pulses as short as 6-femtoseconds[1] and 8-femtoseconds[2] have been produced. Pulses such as these feel the effect of dispersion quite strongly. In order to ensure correct measurements of fast optical pulses, the dispersion of the elements they interact with needs to be known.

A method was introduced to measure the group delay in optical components using an interferometric setup[3]. This group used a narrow band filter with a white light source and tuned the filter to the desired wavelength as the input to a Mach Zehnder interferometer. The element to be measured was place in one arm and the other arm had a moveable platform for a variable time delay. As the delay was varied, the interference pattern was recorded using a photomultiplier. The filter was then tuned to a different wavelength and the interference was scanned again. Group delay was found by comparing the center of the fringe packet with the sample in the arm to a reference scan without the sample in the arm. In order to measure the group delay for different wavelengths, the filter had to be adjusted and then run the scan again. This leads to long measurement times when measuring a wide range of wavelengths and the spectral resolution depended on the wavelength increment between measurements.

To obtain better spectral resolution, another method was demonstrated using phase-locked interferometry[4]. In this method, a tunable source was used with a narrow bandwidth, setting the wavelength resolution[5]. The detector was locked onto a fringe and a feedback loop kept this position by varying the length of the reference arm. As the wavelength of the source was tuned over the range of wavelengths, the optical pathlength

in the sample changed due to a different delay depending on the wavelength. The amount the reference arm had to be moved to compensate for the change in optical path length was recorded and from this data, the wavelength dependent group delay could be found. A drawback of this system is that the source has to be variable over the range of wavelengths of interest.

Another group[6-8] presented a way to measure the group delay of optical components for a wide range of wavelengths from one set of interferometric scan data. A Michelson interferometer is used, but this time a fiber transmitted Xe lamp is used as the wide bandwidth white light source. Again, the element to be measured was inserted in one arm and the other arm was scanned over a delay range. The group delay was then found by taking the derivative of the Fourier phase of the interference pattern and removing delay bias of the system found from a baseline scan with no sample present.

The purpose of this paper is to take a look at the development and characterization of a system that can be used to determine the characteristics of an optical sample by using white light in the infra-red region at wavelengths 1530 nm to 1560 nm. These wavelengths are of interest because a lot of work is currently being done with femtosecond pulses generated by Erbium doped fibers at these wavelengths. The system will eventually be used to study the change induced in the correlation trace as spectral components of the source are altered by means of a pulse shaper in the sample arm.

An Erbium doped fiber pumped by a Ti:sapphire laser was used to generate the white light. The output from this fiber is then fed into a Mach Zehnder interferometer and the interference pattern is recorded using a photodiode and computer. The interferogram is Fourier transformed to yield phase and amplitude information of the interferometric system. The resulting Fourier amplitude should produce the power spectrum of the source[8]. Differences between this calculated power spectrum and the one directly measured with a spectrum analyzer, should give insight whether the interferometer accurately performs the correlation of the light in the arms of the interferometer.

Samples were put into one arm of the interferometer and their effect on the correlation trace was studied.

2. AUTOCORRELATION AND INTERFEROMETERS

When a beam is passed through the beamsplitter in a compensated Michelson interferometer, shown in figure 2.1, it is split into two waves having equal electric field magnitudes. The wave traveling through the sample arm sees a fixed delay and its complex electric field amplitude is written as *E(t)*. The other wave experiences a variable time delay τ determined by the position of a moveable translation stage, and its complex amplitude is written as $E(t-\tau)$. At the output, the resulting complex electric field is the sum of these two fields:

$$U=E(t-\tau)+E(t) \tag{1.1}$$

The power transmitted through the interferometer is the integral of the square of this electric field[9]:

$$Power=\int|E(t-\tau)+E(t)|^2 dt \tag{1.2}$$

Expanding this equation produces:

$$Power=\int|E(t-\tau)|^2 dt+\int|E(t)|^2 dt+\int\left[E(t-\tau)E^*(t)\right]dt+\int[c.c]dt \tag{1.3}$$

The first two terms of equation (1.3) are DC terms which are delay independent and will be ignored for the moment. The important terms are the last two terms which correspond to the interference of the two fields as the delay between the two arms is varied. These terms are also referred to as the complex autocorrelation functions. The two terms are complex conjugates of each other, therefore only one is looked at for now.

Fourier transforming the positive frequency fringe terms results in:

$$\iint E(t-\tau)e^{-j\omega(t-\tau)}E^*(t)e^{j\omega t}dtd\tau \tag{1.4}$$

Rearranging terms produces:

$$\int E(t-\tau)e^{-j\omega(t-\tau)}d\tau \int [E(t)e^{-j\omega(t)}]^* dt \qquad (1.5)$$

Which is: $E(\omega)\, E(\omega)^*$ or $|E(\omega)|^2$, the power spectrum of the input field. The last term of (1.3) produces the same result except at negative frequencies: $|E(-\omega)|^2$ which is just the mirror image of $|E(\omega)|^2$.

If an optical element with transfer function $H(\omega)$ is put into one of the arms of the interferometer, similar analysis shows the spectrum is multiplied by the transfer function:

$$H(\omega)|E(\omega)|^2 + H(-\omega)|E(-\omega)|^2 \qquad (1.6)$$

The transfer function of the optical element can then be found by dividing off the spectrum of the source.

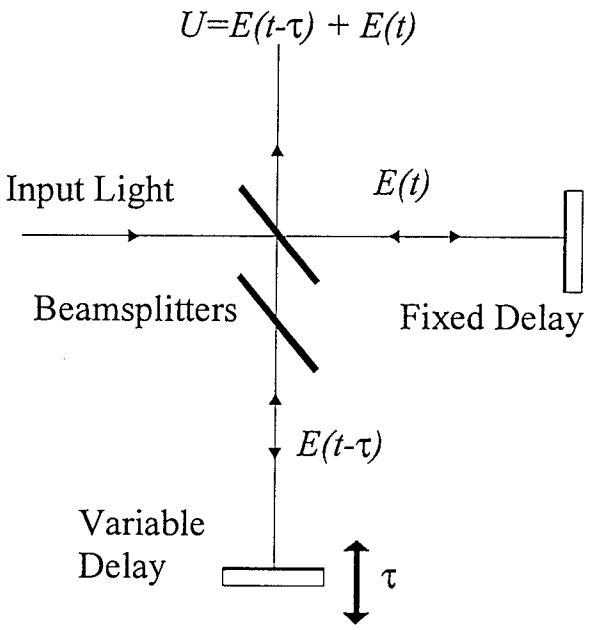

Fig 2.1 A Compensated Michelson Interferometer[10]

3. EXPERIMENTAL SETUP

3.1 INTRODUCTION

Figure 3.1 shows the experimental setup used to measure the group delay of different samples. It consisted of three main parts: the source, the measurement system, and the data acquisition. The source, consisting of a Ti:sapphire laser pumping an Erbium doped fiber, produced the white light which was directed into the interferometer, the measurement system. The interferometer was used to generate an electric field correlation which was then measured using a photodiode and computer(data acquisition).

3.2 PROPERTIES OF ERBIUM DOPED FIBERS

A good source of white light with a wide bandwidth around 1540 nm is the amplified spontaneous emission (ASE) of an Erbium doped fiber[11-13]. When a pump beam from a Ti:sapphire laser at 980 nm is coupled into the Erbium doped fiber, the electrons are excited from the ground state to the pump state($I_{11/2}$). Refer to Figure 3.2. The lifetime of the pump state is very short, about 7 μs, and the electron quickly relaxes down to the upper laser state which has a longer lifetime of about 10 ms[12]. The spontaneous emission then occurs from the upper laser state back down to the lower laser state (ground state). The wavelength of this emission is around 1550 nm.

Also observed in the laboratory and used to optimize coupling of the pump light into the fiber is a green glow from the fiber. The glow can be explained from looking at the figure of the energy levels. An electron which is pumped to the pump state ($I_{11/2}$), can either relax or absorb another photon. Most of the electrons rapidly decay to the upper laser state, but a few absorb another pump photon (excited state absorption) and are pumped to a higher short lived state[12]. These upconverted electrons then radiate back

to the ground state and emit green light around 545 nm which is visible to the naked eye and can be useful when trying to couple infrared light into the fiber. The better the coupling, the brighter the visible emission.

This can be used as a rough maximization for coupling from day to day when maximum output power is not needed.

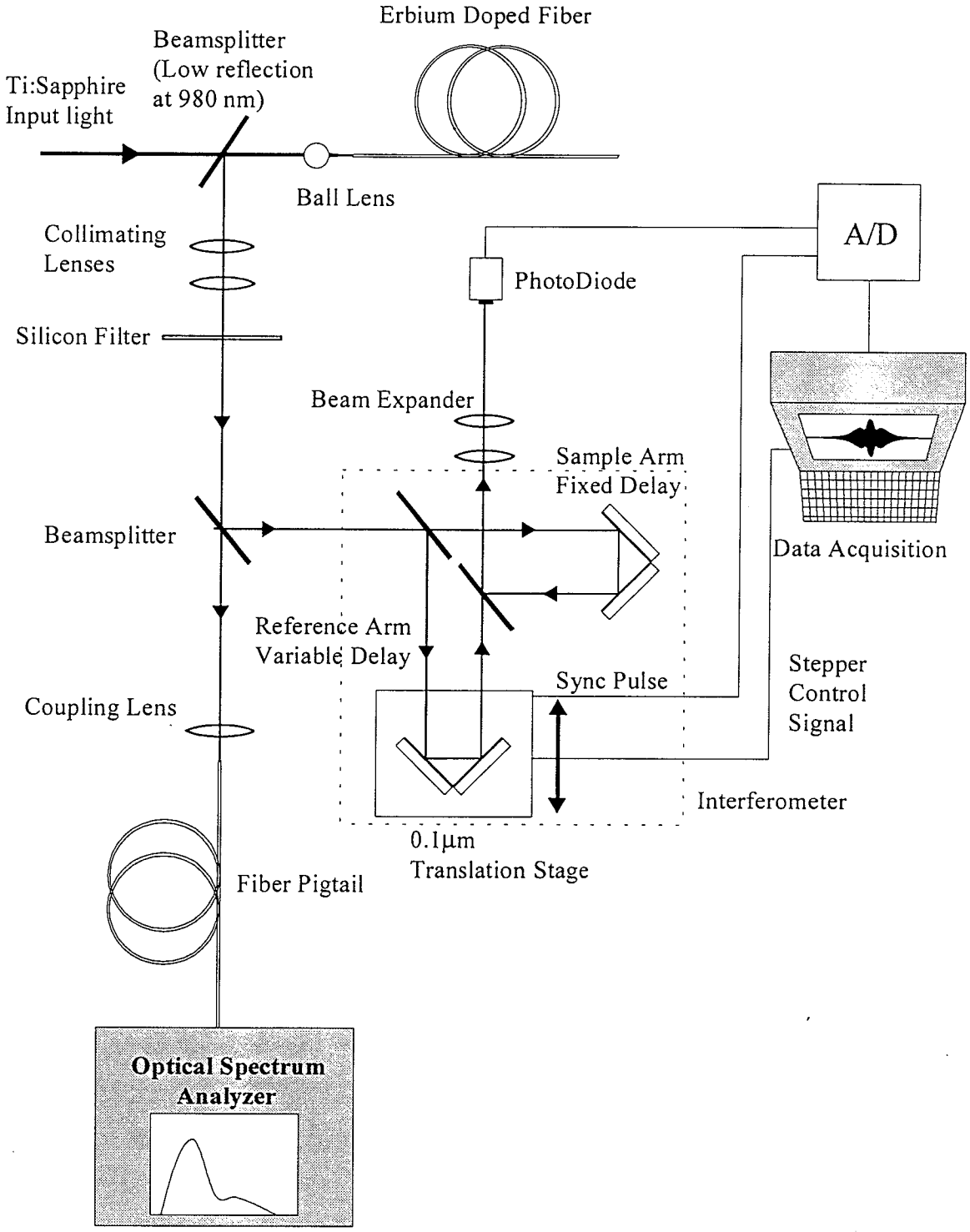

Figure 3.1 Experimental Setup

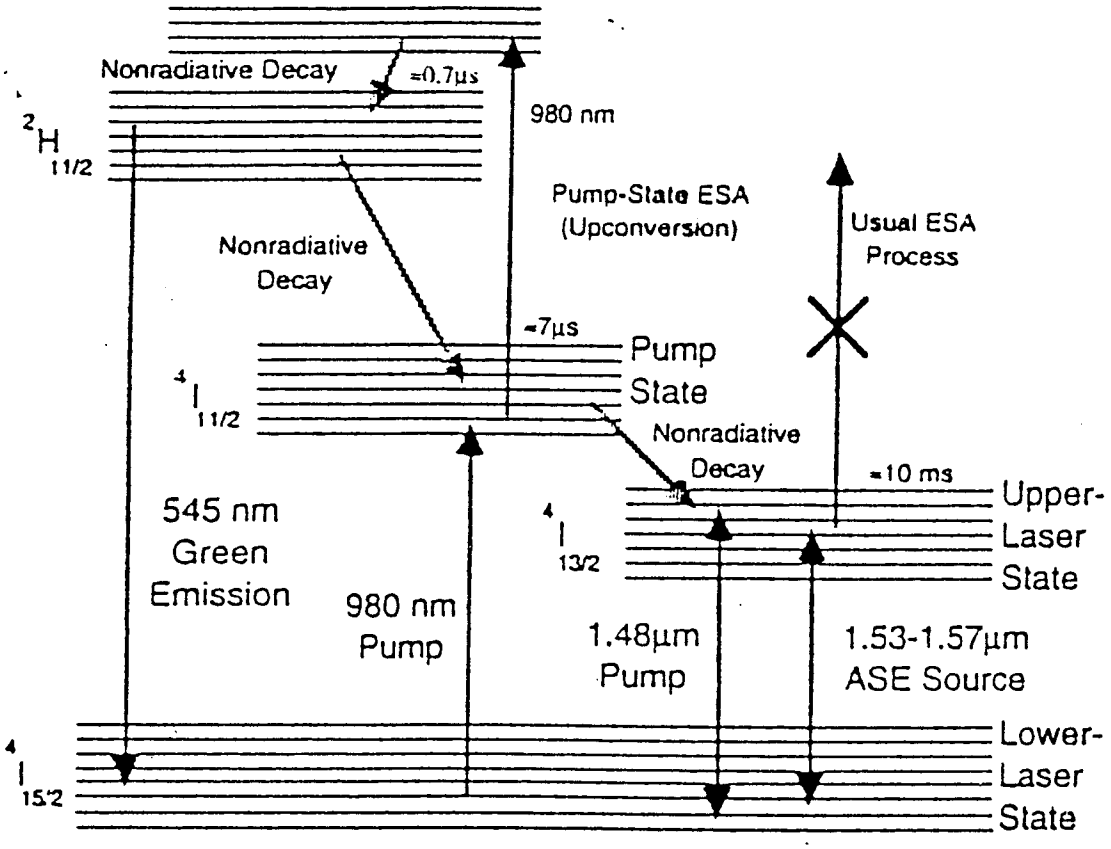

Figure 3.2. Energy Levels for an Er:silica Fiber Pumped at 980 nm[5].

3.2.1 CO PROPAGATING AND COUNTER PROPAGATING ASE

Spontaneous emission will be amplified in the region of the fiber where there is sufficient pump power to invert the electrons. Typically, in long fibers the pump power is not sufficient enough to invert the whole length of the fiber. Spontaneous emission starting at the pump end of the fiber will see gain at the inverted part and absorption then near the unpumped end of the fiber. As the fiber is pumped harder, the effects of absorption on the forward (co-propagating) emission is decreased[11,12]. This can be explained by looking at the loss/gain plot in Figure 3.3. The figure is a plot of typical gain and absorption spectra around 1530 nm.

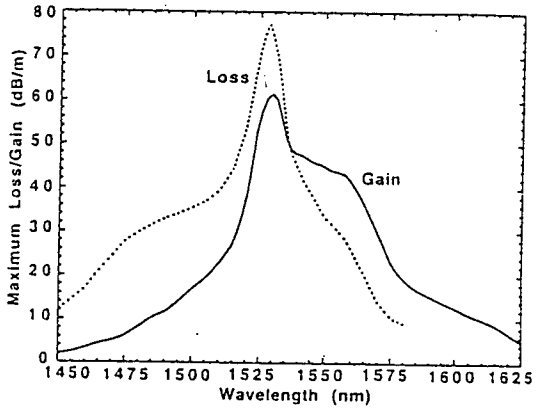

Figure 3.3. Gain/Loss Spectra of a Typical Al:Ge:silicate Fiber[12]

In long fibers, spontaneous emission originating in areas near the pump end of the fiber see high gain. As the light propagates throughout the fiber, it continues to be amplified, most strongly between 1525 nm and 1560 nm which is the region of high gain shown by the fluorescence curve. When the light reaches an unpumped region of the fiber, it is reabsorbed. Looking at the absorption curve, the strongest absorption is seen at 1530 nm. At higher wavelengths, the absorption is much less. As the unpumped region becomes longer, the light sees more attenuation at the lower wavelengths where the strongest absorption peak is, thereby greatly reducing the power at these wavelengths.

This also has an effect of causing a shift in the center of the ASE spectrum to higher wavelengths[12]. The shape of the spectrum will be a filtered version of the gain spectrum where the filter has the shape of the absorption curve. With strong pump powers, the light sees less filtering and has more power left at the lower wavelengths than light propagating through a lightly pumped fiber.

Backward propagating ASE (counter propagating) has its origin somewhere near the middle of the fiber where the pump power just has enough power left to cause inversion. This light travels from a region of low inversion to strong inversion. The light builds in intensity and is similar in shape to that of the gain spectrum. Differing from the co-propagating light, this light does not see a region of high absorption. From this fact, the peak at 1530 nm should not become highly attenuated even at low pump powers. It has been shown theoretically and experimentally that this is the case[11,14].

Output powers for these long fibers increase as the pump power is increased. The backward propagating ASE is stronger than the forward propagating ASE for a given pump power[11,12] because it does not see an area of absorption in an umpumped region of fiber before being emitted.

Emitted spectra of short fibers differs from that of the longer fibers[11,12,14] due to the lack of an unpumped lossy region at the unpumped end of the fiber. In a shorter fiber, the pump has enough power to cause inversion through the whole length of fiber. Forward propagating light sees less of a region of high loss due to an unpumped section of fiber as it did in a long fiber. The powers measured for both the forward and backward propagating ASE are similar in magnitude. As the pump power is increased, a point is reached where the effect of absorption vanishes and the two powers are equal. As the power is increased further, the outputs saturate because of bleaching of pump absorption[12]. This is different than in long fibers where the output power keeps increasing with increasing pump power[11].

The definition of a short fiber and long fiber is rather subjective. A short fiber can be considered one in which the forward propagating ASE sees minimal if any, absorption because the fiber is completely inverted. This length, however, is strongly dependent on

input pump power, coupling efficiency, and doping concentration. Higher pump powers will cause inversion over a longer region of fiber than low pump powers. A weakly pumped fiber with an umpumped lossy region at the far will exhibit behavior of a long fiber: the peak at 1.53 μm being strongly absorbed. Pumping the same fiber harder might cause the whole fiber to see inversion and then it would exhibit characteristics of a short fiber. For a given pump power, increasing coupling efficiency will put more power into the core, thus increasing the length of gain. Again the same fiber could exhibit behavior of a long or short fiber depending on the input conditions. The heavier doped the fiber is, more pump photons are absorbed per unit length decreasing the length of fiber seeing inversion. Thus, a heavily doped fiber will seem longer than a lightly doped fiber of the same length.

3.2.2 EXPERIMENTAL SOURCE

The experimental setup to measure the forward and backward propagating ASE is shown in Figure 3.4. The fiber used was 5 meters of an Erbium doped Germania Calcia-alumina Silicate core fiber from Bellcore. Core size of the fiber was 3 μm and attenuation was reported as 8.0dB/meter @ 980 nm. The index difference was $\delta n=0.017$ and the cut-off wavelength was 0.9 μm[24]. Based on the high attenuation, fiber length used, and discussion in section 3.2.1, this fiber should exhibit characteristics of a long fiber. Thus, the spectral shape of the forward propagating ASE should change with input power, especially near the 1530 region of high loss.

Ti:sapphire pump light was coupled into the 5 meters of Erbium doped fiber using a Melles Griot 5 mm fiber coupling sphere anti-reflection coated at 980 nm. Coupling efficiencies of these lenses are quoted as 95% for coupling into standard communication fibers. The coupling efficiency achieved in this setup could not be found without some way to directly measure the light coupled into the fiber core. A colleague[15] used the same coupling sphere and fiber and reported typical coupling efficiencies of 40%. This measurement was done by splicing a 90/10 coupler into the fiber at the input and the amount of power actually coupled into the core was measured. The 40% coupling

efficiency is not a reliable estimate for the coupling into the fiber in this experiment because of differences in core sizes. The 90/10 coupler had a core diameter of 9 μm whereas the core of the Erbium fiber used here was 3μm. With a smaller core, the coupling efficiencies would be much less as it is much harder to couple light into a smaller core.

To increase lasing threshold, the unpumped end of the fiber was angle cleaved at about 10-15% to suppress feedback off the end of the fiber. Any light reflected off the end of the fiber would act as an injected signal and be amplified as it traveled through the fiber. Suppressing this reflected light allowed the fiber to be pumped harder before it started lasing, thus emitting more ASE power[12].

No output power data was not taken for the 5 m fiber with a flat cleave to show this, but a 4 m fiber used prior to the 5 m fiber showed an increase in the lasing threshold from about 80 mW to about 250 mW resulted after angle cleaving. These numbers cannot be taken at face value however. The power measurements with the flat end were taken a different day than the measurements with the angle cleave. Coupling efficiencies varied widely from day to day, and without some way to measure the exact amount of power coupled into the fiber, as mentioned earlier, the exact percentage increase for threshold could not be determined. Allowing for a reasonable difference in coupling efficiencies between the two days, a significant increase in the threshold can be seen.

The forward propagating ASE emission from the fiber was collimated by another spherical lens anti-reflection coated at 1550 nm. To view the spectrum of the light, it was coupled into a fiber pigtail and displayed on a spectrum analyzer. The ASE power was found by placing a photodiode before the fiber pigtail and reading the measurement off a calibrated oscilloscope.

A 22.5 mil(0.572 mm) thick Silicon wafer polished on both sides was placed between the output of the fiber and the measurement apparatus. The purpose of this wafer was to block any of the 980 nm pump light that might have bleached its way through the fiber and would lead to erroneous output power readings.

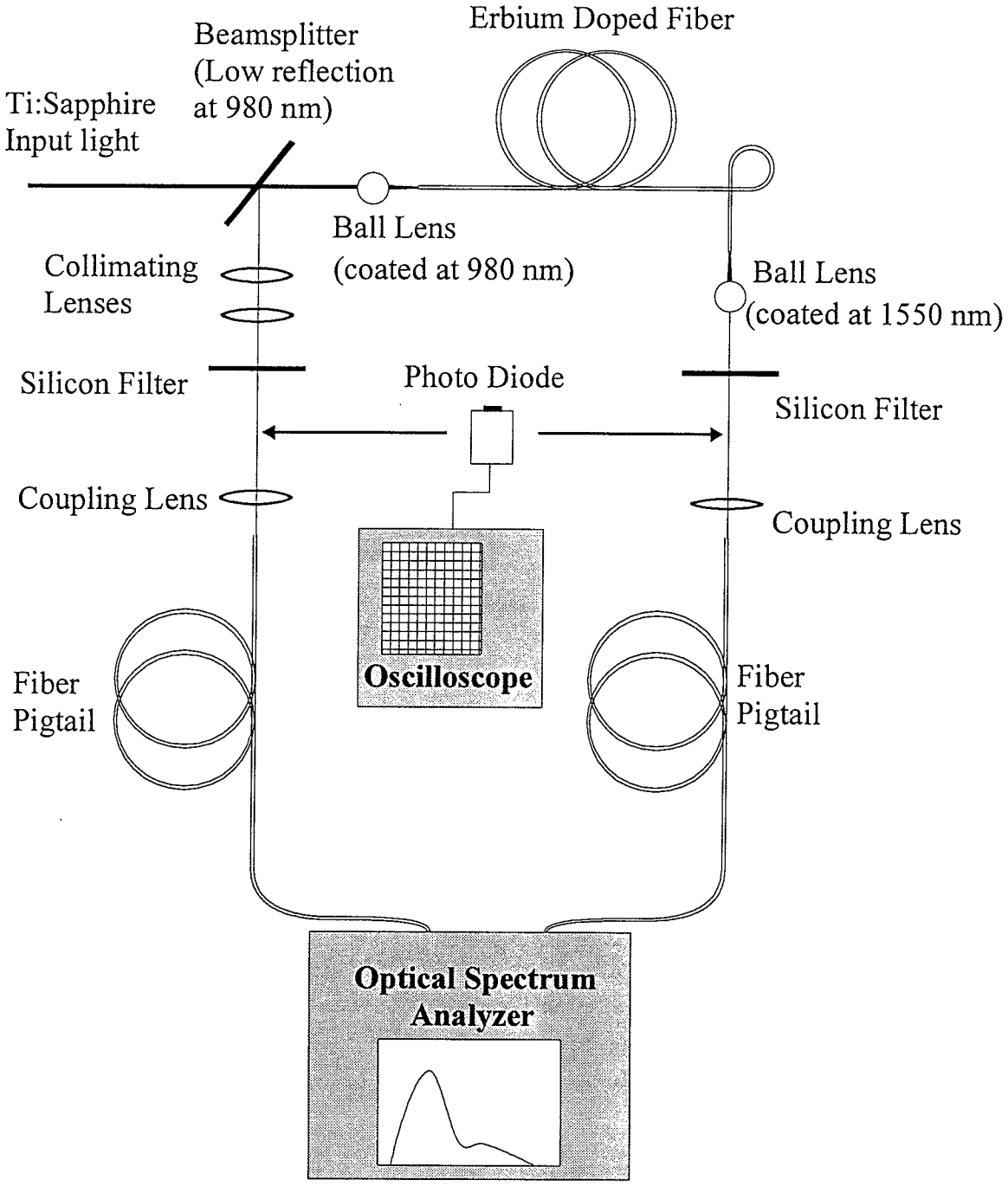

Figure 3.4 System to Measure ASE

A beamsplitter was placed in front of the input end of the fiber to reflect the backward propagating light into a similar setup to measure its power and spectrum. The beamsplitter was coated to be 50% transmission and 50% reflectance at 1550 nm, but was highly transitive at 980 nm to pass most of the pump beam to the fiber. ASE power readings from the oscilloscope for the backward propagating ASE had to be multiplied by a factor of 2 to account for the loss of power through this beamsplitter.

Output powers versus pump powers for both co-propagating and counter propagating light are shown in Table 3.1.

Output spectra for co-propagating ASE are shown in Figure 3.5. Pump powers incident on the ball lens before coupling for these spectra are 90 mW, 100 mW, and 120 mW.

Counter-propagating spectra are shown in Figure 3.6 for the same pump powers.

Table 3.1

Counter and Co-propagating ASE Powers for Varying Pump Powers

INPUT		Co		Counter
90mW		0.97mW		2.16mW
100mW		1.2mW		2.4mW
120mW		1.62mW		3.0mW

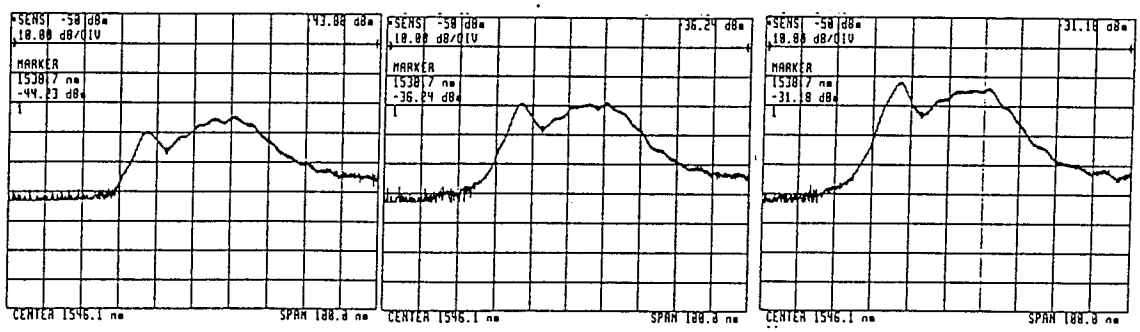

Figure 3.5. Plots of Co-Propagating ASE for Increasing Pump Powers.

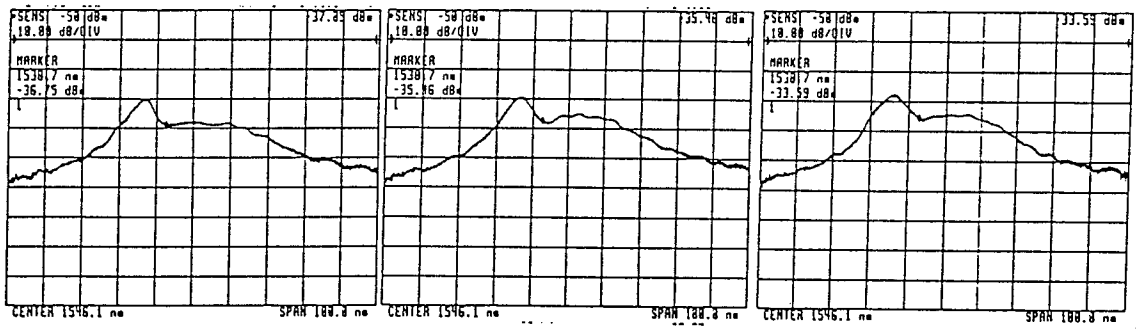

Figure 3.6. Plots of Counter-Propagating ASE for Increasing Pump Powers.

3.2.3 ANALYSIS OF SOURCE

The shape of the spectra in Figures 3.5 and 3.6, changed as predicted by discussion in section 3.2.1 and references[15,19] for long fibers. Increasing pump power induced inversion and thus more gain over a longer region of the fiber.

As seen in Figure 3.6, this had little effect on the shape of the ASE spectrum for counter propagating light. The power, however, did increase with increasing pump power, shown in table 3.1.

Significant changes were seen in the spectra for co-propagating ASE though. The traces in Figure 3.5 are shown on a log scale and therefore are not visually dramatic as if plotted on a linear scale. As the pump power was increased, the peak at 1530 nm could be seen to increase dramatically. With higher pump powers, less of the fiber became unpumped and the forward propagating ASE saw less absorption, specifically at wavelengths around 1530 nm where the absorption peak is the highest. The power output increased with pump power, but not as dramatically as the counter-propagating ASE power.

Comparing the output ASE powers listed in Table 3.1, the power from the backward propagating ASE was about twice that of the forward propagating ASE as shown in other work[11-13,20]. This can be attributed to the fact that the counter-propagating light did not travel through any region of high loss.

Also noted and consistent with other research[11] was the overall percentage increase in ASE powers versus pump powers. An increase of 33% in pump power showed a 67% increase in co-propagating power and an increase of 38% for the counter propagating power. The significant difference in power increase can be attributed to the fact that as the pump power was increased, the unpumped region of attenuation at the end of the fiber was shortened, thereby reducing the attenuation of the forward propagating signal. This had the effect of not only increasing the ASE generated but also of reducing the loss it saw. The backward propagating power increased almost linearly with the pump power because it did not travel through this region of loss. Therefore any increase or decrease in the umpumped length of fiber did not greatly affect it.

A close comparison between the spectra for the two directions reveals the counter-propagating light to have a wider spectral width. This holds with the findings in [12,13]. The additional width of the counter propagating spectrum is seen at the lower wavelengths. A look at the absorption/gain curve will explain. The absorption curve extends to lower wavelengths then the gain curve does. In the co-propagating case, the power in these lower wavelengths is reabsorbed thereby narrowing the bandwidth. The light going in the counter propagating direction does not see the high absorption at these wavelengths and the power in these lower wavelengths is not attenuated as much.

Enlarging one of the spectra and plotting on a linear scale in Figure 3.7, reveals two modulations present. These are due to Fabry Perot cavity effects between experimental components. The small ripple is found to have a $\delta\lambda$ of about 0.58 nm which corresponds to a δf of 73 Ghz. The index of refraction for the Silicon wafers is about 3.6[16], which leads to a cavity length of $d = c/2n\delta f = 0.56$ mm. The thickness of the Silicon wafers is 0.572 mm which matches up pretty closely to this measurement considering the accuracy of reading the period of the oscillation off the figure.

The modulation with a larger period has a $\delta\lambda$ of approximately 4.8 nm. which corresponds to a δf of 600 Ghz. The cavity length is found to be $d = c/2n\delta f = 0.25$ mm which is the focal length of the pump coupling sphere. The end of the fiber and the coupling sphere are acting as a cavity. The reason that the modulation is small is due to the convex surface of the ball lens causing the cavity to be unstable. The power drifts out of the cavity instead of building up.

A few milliwatts of ASE was desired for the light source for the interferometer. The five meter fiber produced enough power to meet this need, and the counter propagating ASE was chosen to be used as this source.

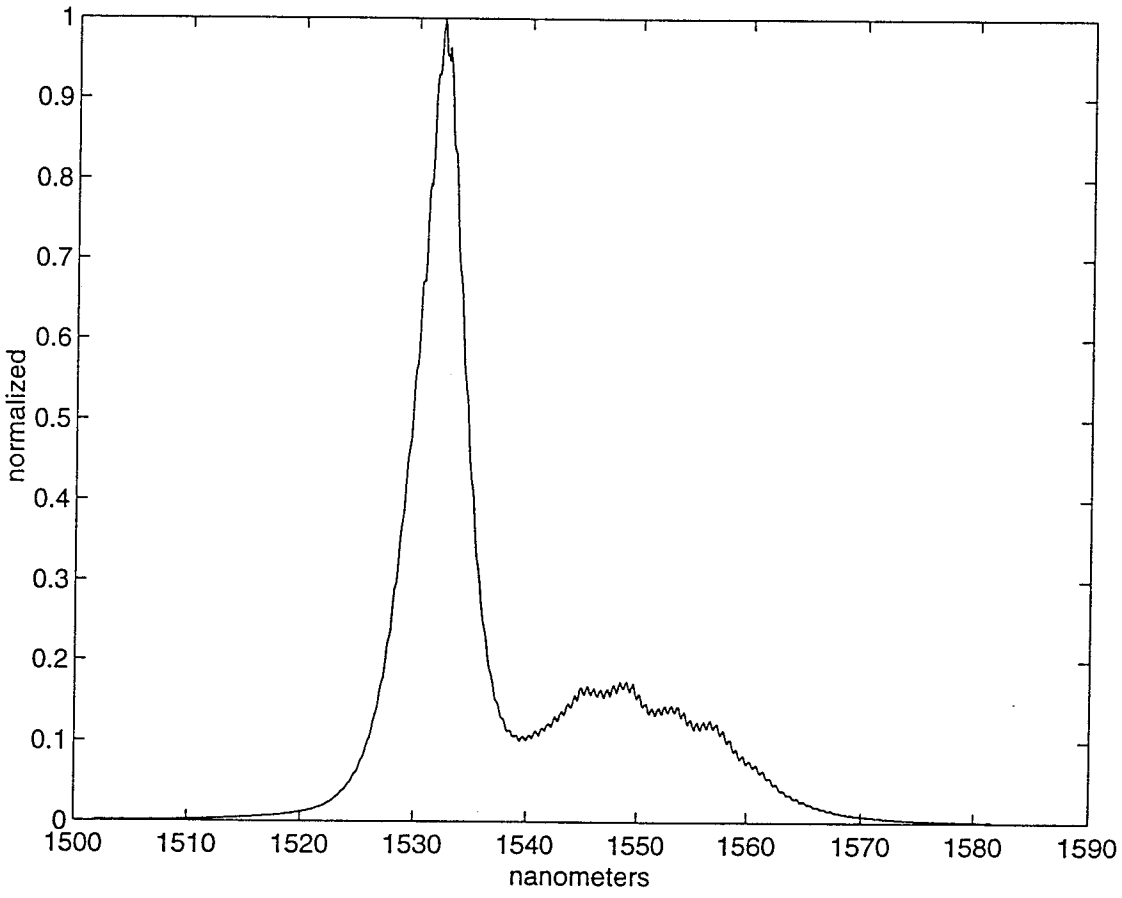

Figure 3.7 Linear Spectral Plot of Counter Propagating ASE

3.3 INTERFEROMETER

The interferometer used in this experiment was a Mach Zehnder interferometer shown in Figure 3.7.

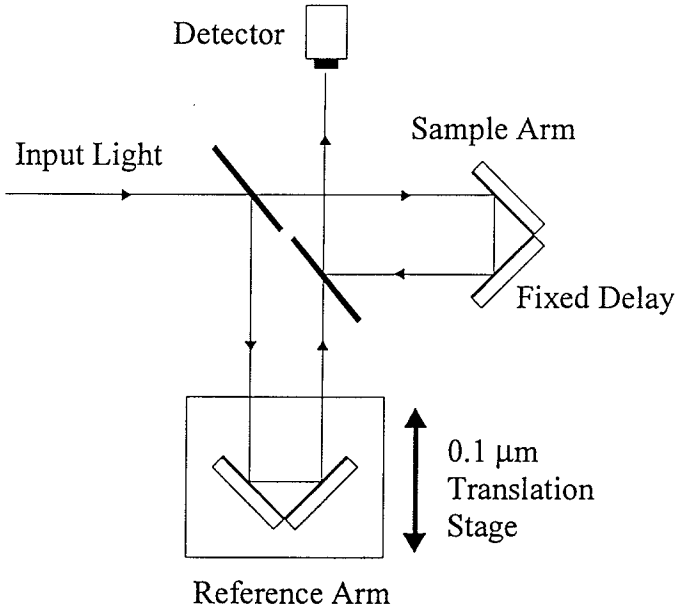

Figure 3.8. Mach Zehnder Interferometer For Electric Field Autocorrelation

The arm in which the sample was placed is a fixed length set by the position of the two non-moveable mirrors. The other arm is the reference arm with a variable delay determined by the position of the translation stage. The two mirrors of the reference arm are placed on a computer controlled translation stage with a step size of 0.1 μm. The actual optical path difference per step was 0.2 μm since the beam transversed this length in one direction, hit the mirrors, and covered the length again going in the opposite direction. Converting to time, each step then corresponded to a 0.667 fs delay, which set the resolution of the electric field correlation measurements. The period of the correlation fringes was about 5.1 fs which allowed between 7 and 8 samples to be taken per fringe.

Other groups using interferometric scans to measure the effects of optical components in the sample arm[3-7,19], used a compensated Michelson interferometer as shown earlier in Figure 2.1. One problem with this arrangement is after retro-reflection, a portion of the light is transmitted back through the beamsplitter as well as reflected to the detector. A potential consequence of this type of interferometer if used in this system, would be this light being coupled back into the Erbium fiber source. Acting as an injected signal, the light would be amplified as it propagated through the fiber and could cause the fiber to lase at a lower pump power. To compensate for the lasing, the pump power would have had to be reduced to bring the fiber back below threshold, thereby reducing the total ASE output power.

A Mach Zehnder interferometer, on the other hand, has two beamsplitters. One splits the beam into the reference arm and sample arm, and the second beamsplitter recombines the two beams after traveling through the arms. The phase of the two arms are balanced owing to the fact that at the second beamsplitter, the light that was reflected from the first is now transmitted in the second, and vice versa for the other beam. The presence of the second beamsplitter also alleviates the feedback into the source because the light transmitted through the beamsplitter is not coupled back into the fiber as might have happened in a Michelson interferometer.

3.4 DATA CAPTURE

A photodiode connected to an oscilloscope was placed at the output of the interferometer to capture the interference fringes. Due to the large surface area of the diode, and small fringe period, many fringes were incident on the detector. This was the result of a slight misalignment of the two beams. They didn't overlap perfectly which would then place the center of the fringe pattern on the detector. A beam expander was placed in the path between the output of the interferometer and photodiode to reduce the number of fringes incident on the detector.

The optical path delay τ between the two arms of the interferometer was determined by the position of the translation stage. The stage was controlled by the same computer

that acquired the interference data. Software was used that scanned the stage over a delay range and stored the measurement from the diode at each step.

The output of the diode was fed into and A/D board on the computer, which sampled the analog output from the diode and sent it to the computer to record. A sync pulse from the translation stage triggered the A/D board to sample at every step.

The software allowed sampling to be done bi-directionally or uni-directionally. Bi-directional means samples are recorded as the stage is scanned in both directions. Uni-directional scanning means the samples are recorded as the stage moves in one direction only.

Figure 3.9 shows an interferogram obtained from a single pass bi-directional scan. The x axis is time and the y axis is in sample units. Comparison to the single pass, uni-directional scan in Figure 3.10 shows the fringe pattern in the bi-directional scan was 'washed out.' What happened was the values sampled for a given delay value were different depending on the direction the stage was moving. Some values added constructively to the previous sampled values, and some added destructively resulting in an erroneous interferogram. A possible cause for this could be backlash, or a slight slippage of the translation stage or mirrors mounted on it as it changed direction.

The uni-directional scan in Figure 3.10 was from one pass only so there could be no washout. This scan, however, shows the presence of a lot of noise seen as random peaks throughout the scan. This noise could be from stray air currents, building vibrations, or laser fluctuations. To help average out this noise, multiple scans were used. Figure 3.11 shows a uni-directional scan measured over 6 scans. Again, the x axis is time, and the y axis is sample units. The noise peaks were suppressed in reference to the interference pattern, and the washout seen in the bi-directional scan was not present.

The peak height for the scan in Figure 3.11 is 1150 sample units which is about six time that of the peak height of 190 for the single scan, confirming the fact that washout was not present. Comparing the peak power to average power in each scan will also show that washout did not occur. For both scans the ratio of peak power to average power is 1.7.

A note on convention used in this paper. In all the scans presented, the x axis is in units of time unless otherwise noted. Zero corresponds to both arms of the interferometer being the same length. A negative time on the scan plot corresponds to the translation stage moving away from the beamsplitter which increased the path length of the reference arm and produced a positive delay. Similarly, a positive time on the plot corresponds to a negative time delay of the light, or a shorter path length in the reference arm.

Spectral resolution was very important. From sampling theory[17], the distance between frequency sample points(δf) after Fourier transforming was determined from the sampling period T. This relationship is $\delta f=1/T$. To achieve better resolution(smaller δf), the sampling period should be extended. The ideal sampling period is from negative infinity to infinity, but this is not practically achievable. With a step size of 0.1 μm, a 4 ps delay will consist of 6000 samples. A greater delay time yields better spectral resolution but also requires a larger number of samples. Due to memory limitations of the data acquisition PC, the limit of samples was 15,000 samples. This corresponds to a delay of 10 ps and a resolution of 100 Ghz. Scans of 8 ps (δf=125 Ghz) were usually used since longer scans yielded no new data owing to the fact that the tails of the scan averaged out to zero beyond about 3 ps either side of the main lobe as seen in Figures 3.9-3.11. If better spectral resolution was required, the data could be padded with zeros before calculations were made.

At the same time the interference scan is taken, another computer captured the spectrum from an optical spectrum analyzer. This data was used to compare the results of Fourier transforming the scan. As mentioned earlier, the Fourier transform of the electric field correlation performed by the interferometer yields the power spectrum. Taking the data from a scan and Fourier transforming it, should produce a spectrum that resembles the spectrum sampled from the analyzer. A close agreement between the two would confirm that the scan is an accurate electric field correlation free from noise or unwanted errors.

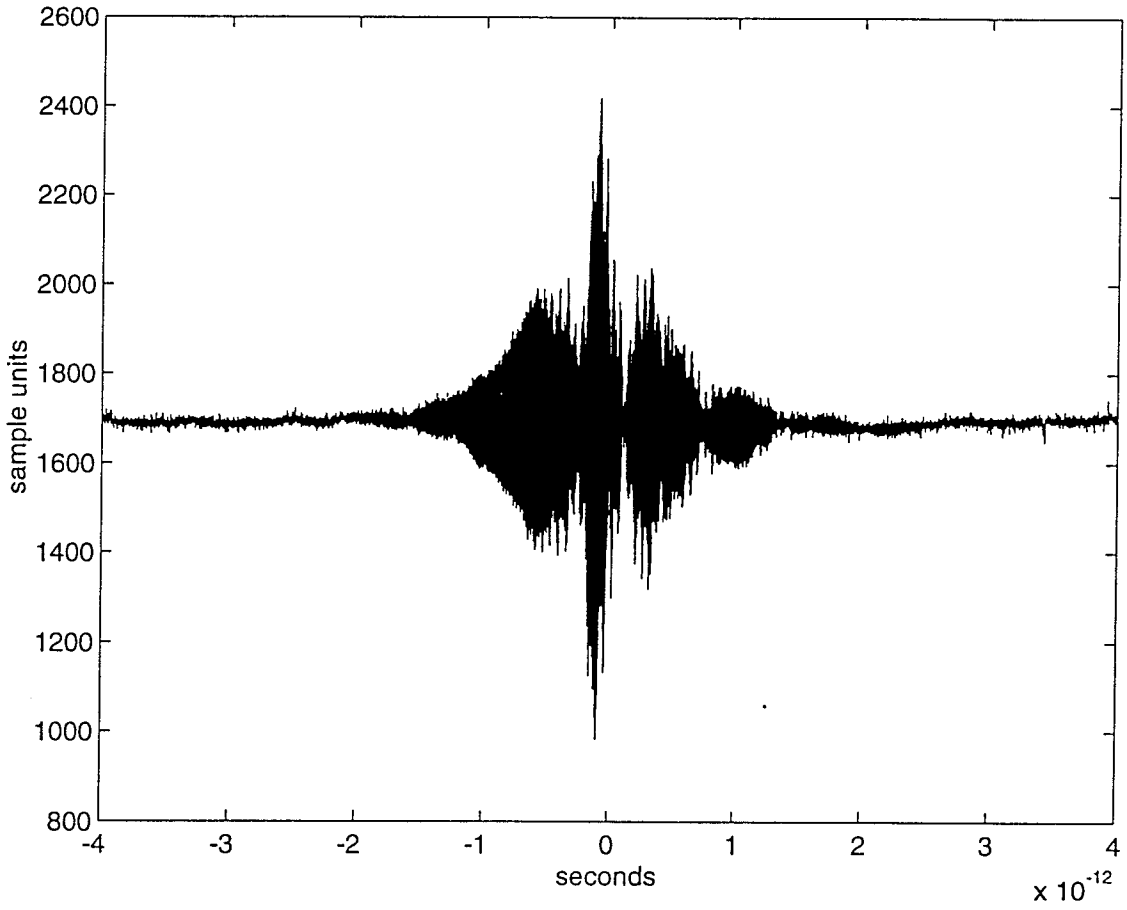

Figure 3.9 8 Picosecond Bi-Directional Scan Showing Washout of Fringes

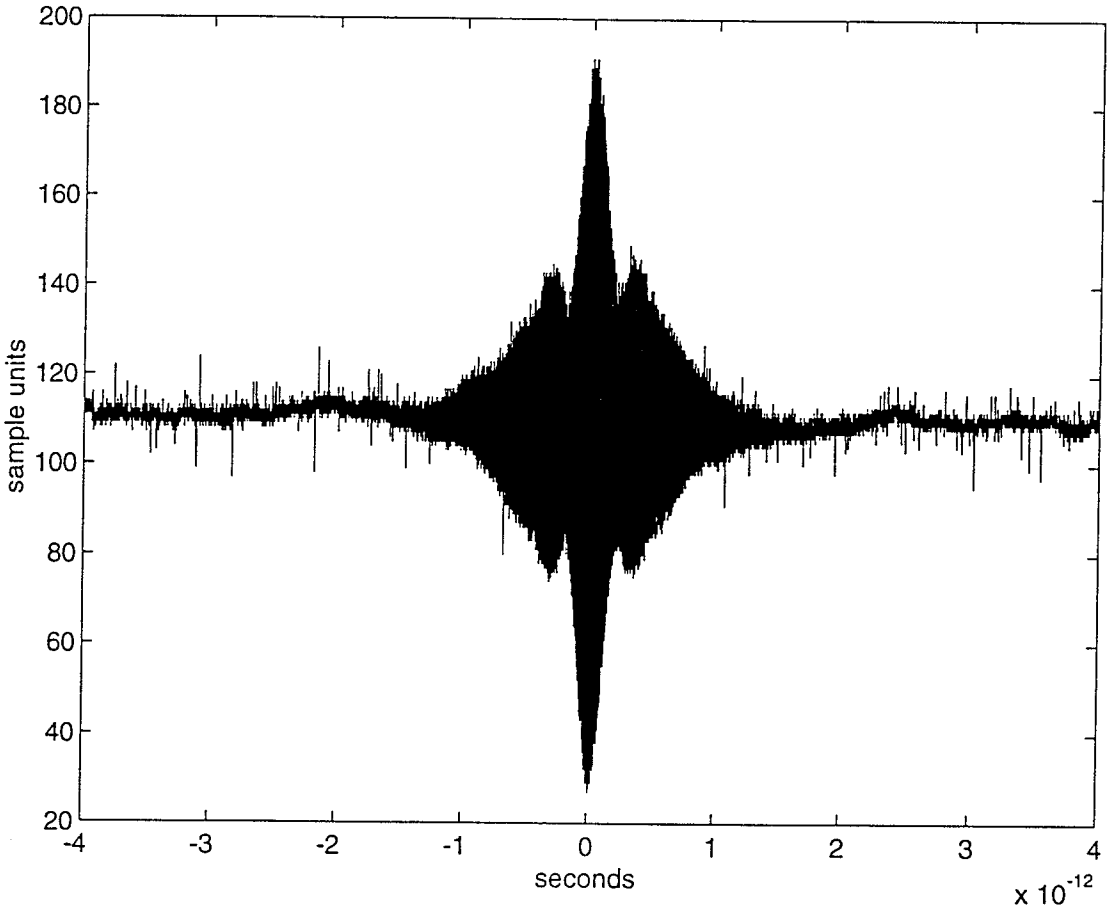

Figure 3.10 8 Picosecond One Pass Uni-Directional Scan.

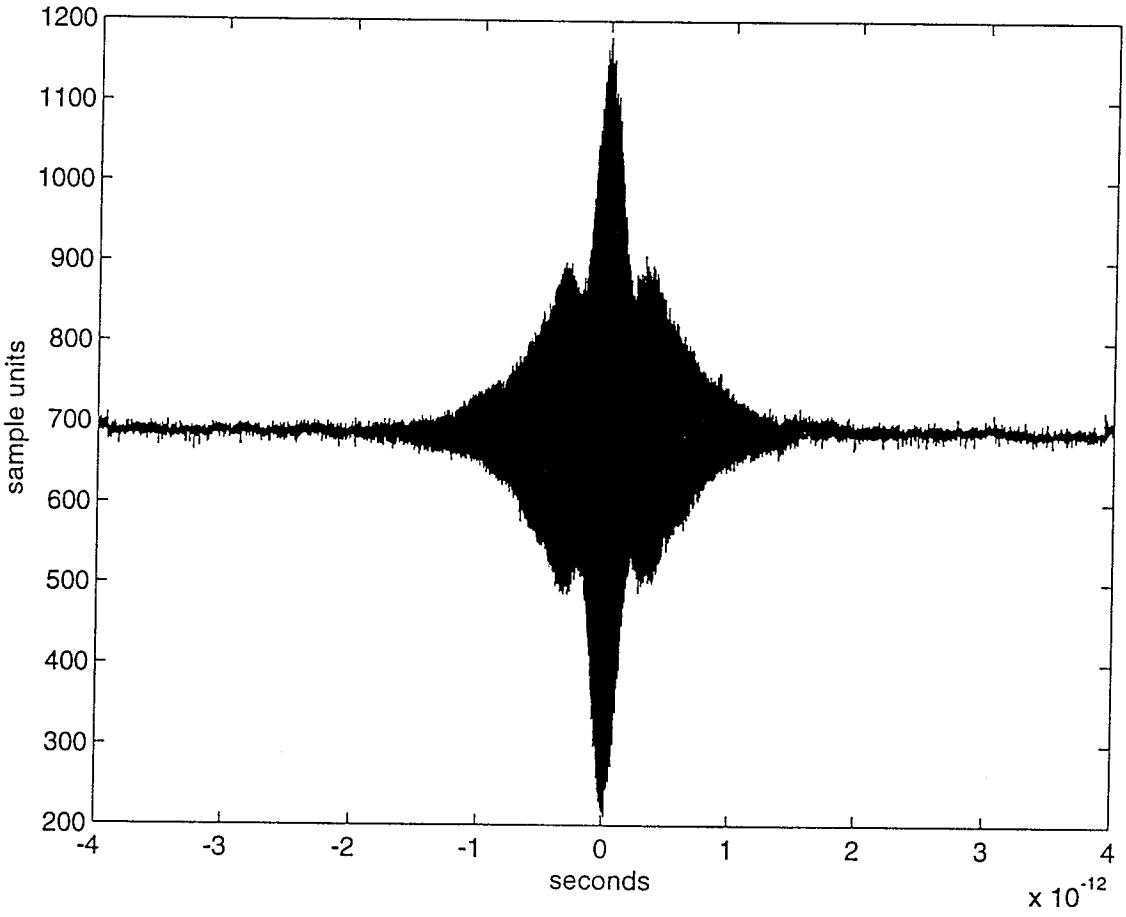

Figure 3.11 8 Picosecond Six Pass Uni-Directional Scan

4. DATA MANIPULATION AND ANALYSIS

4.1. TRANSFORMATION AND COMPARISON OF DATA

Figure 4.1 shows the same interferogram measured over six scans as shown in Figure 3.11, except the dc offset was removed by subtracting off the mean of the data and the amplitude was normalized with respect to the peak power.

For convenience, the data acquired this day will be refered to as Experiment A.

As discussed in chapter one, the Fourier transform of the correlation should produce the power spectrum of the source. There should be two copies, one at positive frequencies and one a negative frequencies. The data shown in Figure 4.1 was transformed by computer and the result is shown in Figure 4.2. The y axis is arbitrary units, but the x axis is frequency. The span of the plot is 1500 Thz ranging from -750 Thz to 750 Thz. The span of the transform data was determined by the sample resolution which was 0.667 fs per step.

$$F = \frac{1}{\delta t} \tag{4.1}$$

The frequency range that spans the source light is a 10 Thz band centered at 195 Thz. This section of Figure 4.2 is plotted in Figure 4.3 with the amplitude normalized with respect to the peak power and the x axis converted to wavelength. Also plotted in Figure 4.3 is the normalized power spectrum obtained directly from the optical spectrum analyzer.

The two spectra are similar in shape with two major differences. One difference is the hump centered at 1550 nm is more pronounced in the calculated spectrum. The other is the presence of an extra hump at 1523 nm in the calculated spectrum. The origin of these two differences has not been determined at this time.

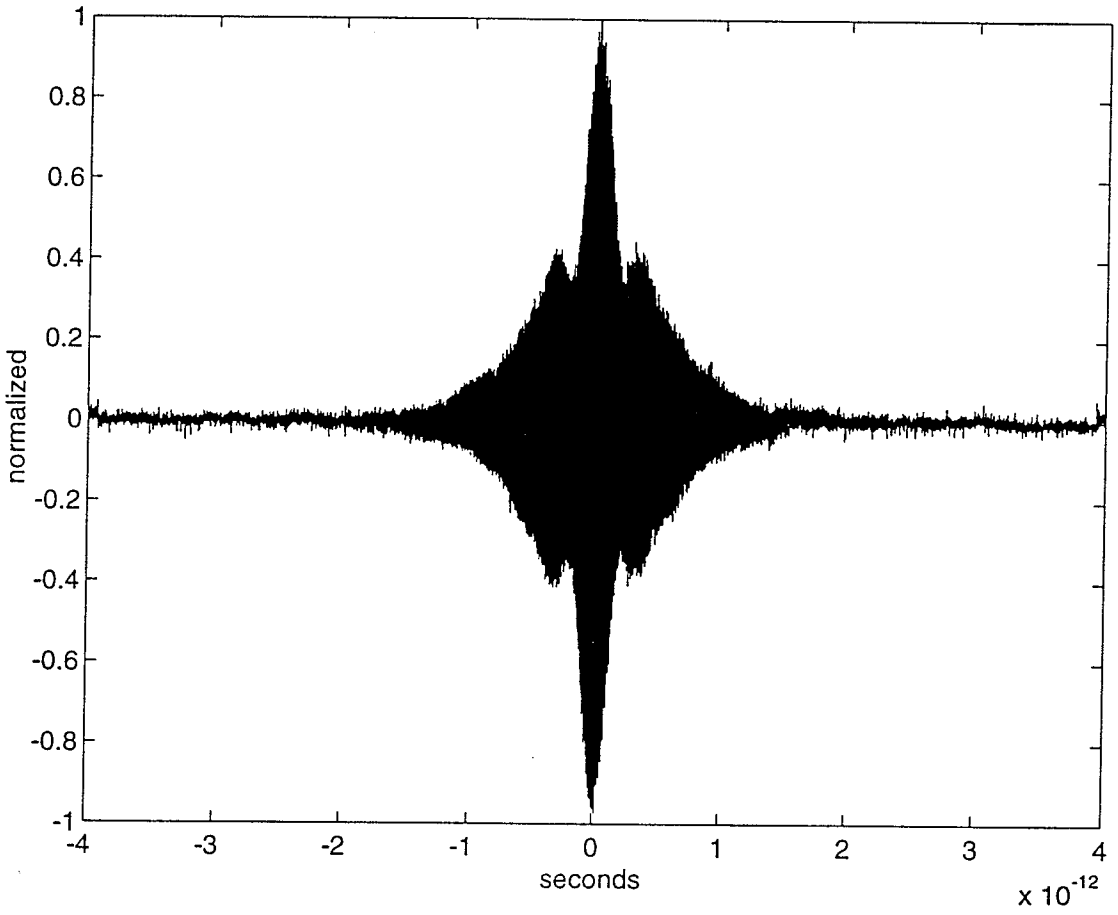

Figure 4.1 8 Picosecond Six Pass Scan Normalized

Experiment A

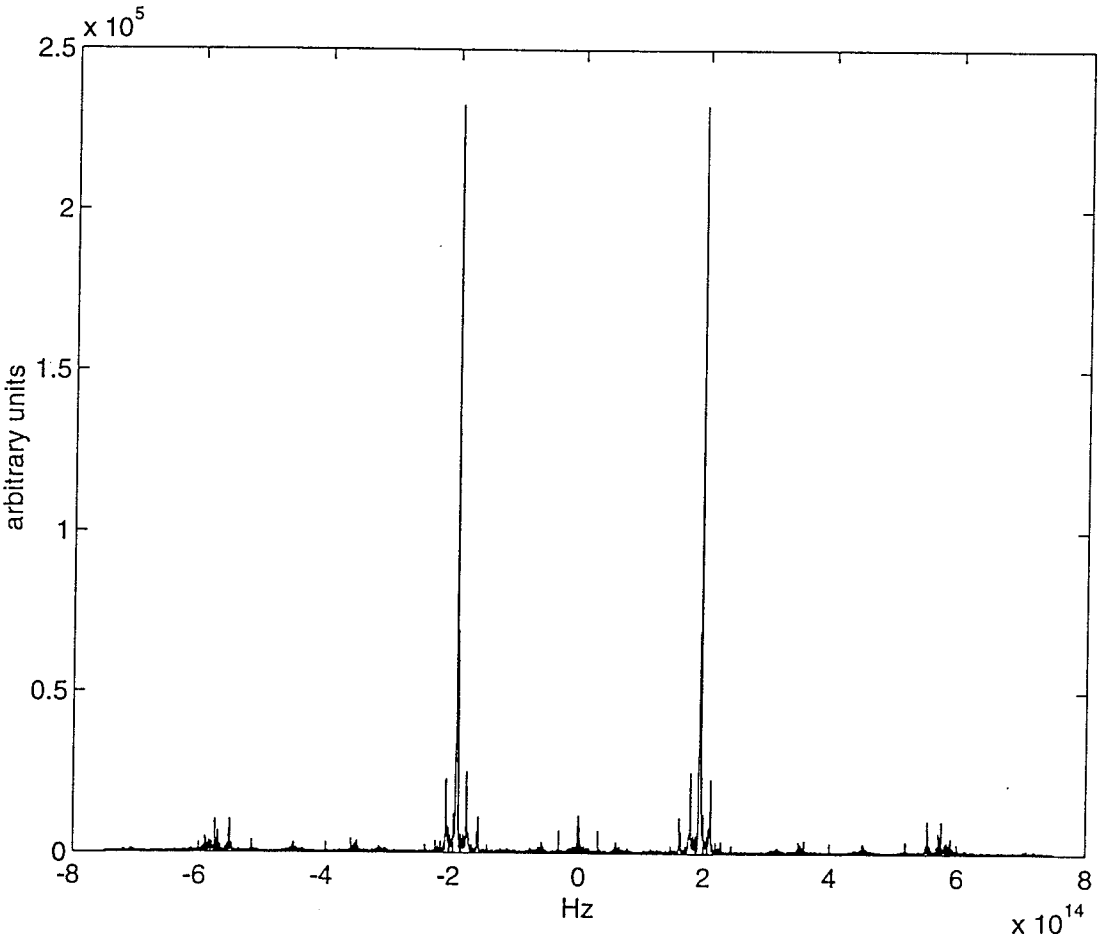

Figure 4.2 Plot of Fourier Transform of Figure 4.1

Experiment A

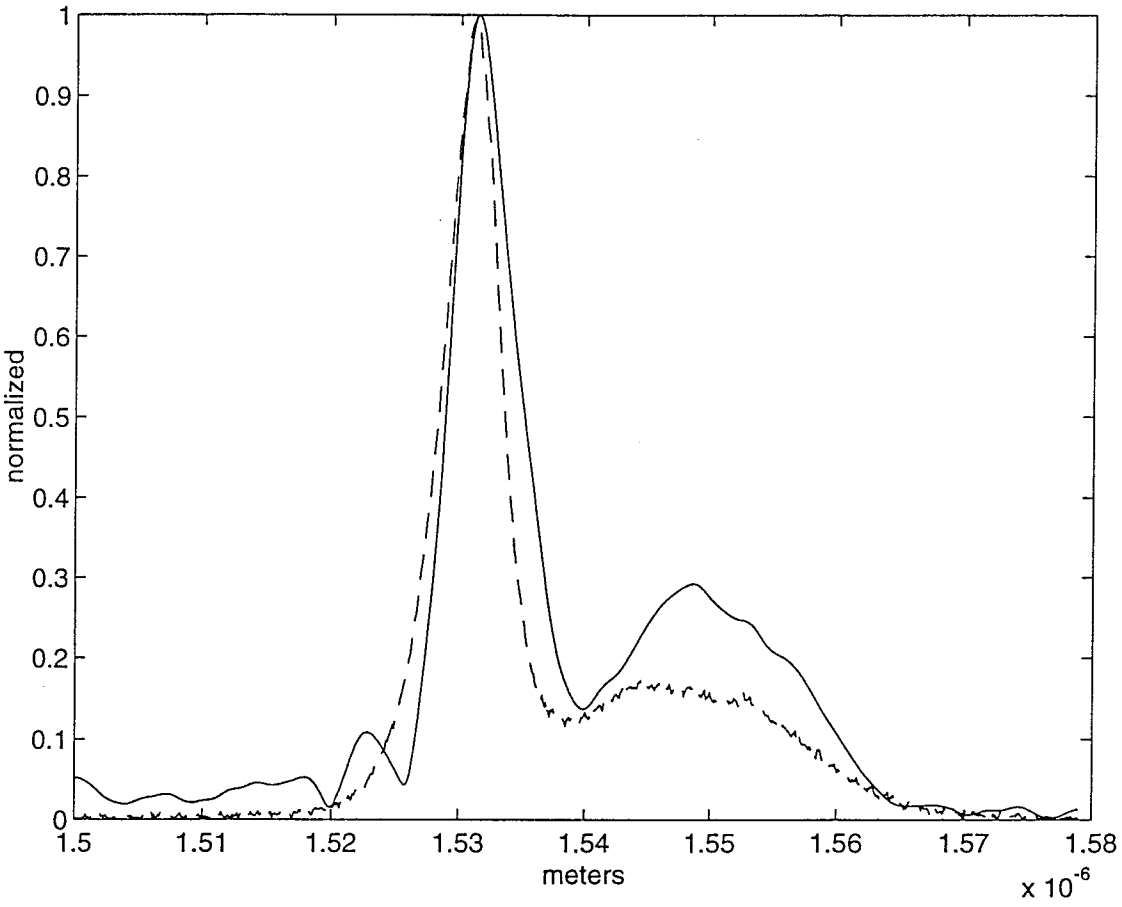

Figure 4.3 Plot of Measured Spectrum(--) and Calculated Spectrum(-)

Experiment A

Figure 4.4 shows a single pass scan acquired on a different day than the data previously dicussed for Experiment A. The data presented from this day will be refered to as Experiment B.

The powers of this scan as compared to the single pass scan in Figure 3.10 are about two and a half times larger. A reason for this could be that the output of the light from the erbium fiber was higher this day due to a higher pump power or better coupling.

A beam expander was not used before the photodiode on this day and the result was more fringes incident on the detector. This reduced the extinction ratio which is defined as maximum power/minimum power to about 3.7 which is a little over half that seen in Figure 3.10 for Experiment A. A lower extinction ratio means less contrast in the interferometric data recorded and less accuracy in the data.

Figure 4.5 shows a uni-directional scan measured over 6 passes without the beam expander. Again, washout was not present in these scans as the peak power for 6 scans is about 6 times that of the single scan in Figure 4.4. The ratio of the peak powers to average powers in these scans is also constant at 1.6.

The scan in Figure 4.5 is shown in Figure 4.6 with the dc offset removed and normalized to the peak power. The Fourier transform of this scan is shown in Figure 4.7 along with the measured spectrum from the spectrum analyzer.

Significant differences are seen between the two spectra. The most notable are the lack of the dip in the spectrum at about 1538 nm and the width of the main peak being much wider in the calculated spectrum.

The spectrum calculated spectrum from this day varies significantly to that from Experiment A shown in Figure 4.3. Insight as to why the two calculated spectra are so different can be gained by looking at a comparison of the experimental correlation data to the theoretical correlation data obtained by inverse Fourier transforming the measured spectrum.

To properly compare the experimental data for the different days, a measured spectrum is used from the corresponding day.

Figure 4.8 shows the theoretical electric field correlation plot calculated from the measured spectrum in figure 4.3 for Experiment A. This correlation pattern is used to compare the experimental correlation pattern in Figure 4.1 Figure 4.9 is the theoretical correlation obtained from the measured spectrum in Figure 4.7 for Experiment B. These theoretical scans were then plotted on the same plot as their corresponding experimentally recorded correlation fringe pattern. The view was zoomed in to see the details of the fringe patterns.

Figure 4.10 shows a blow up of the fringe pattern for Experiment A. The x axis is zoomed into the section from 0.1 ps to 0.3 ps. The theoretical correlation is shown as the solid line and the experimental correlation is the dashed line.

Figure 4.11 shows a blow up of the same time frame for the correlation scans of Experiment B.

Both the experimental correlation traces wander off from the thoeretical traces but the trace for Experiment B wanders off farther because of larger phase errors. The correlation in Experiment A also deviates slightly from the thoeretical trace in the time slot of Figure 4.10, but another time slot from 0.7 ps to 0.9 ps (Figure 4.12) shows this trace to match up almost perfectly to the theoretical trace. A different situation is seen for Experiment B in Figure 4.13. The correlation trace keeps wandering farther off as the delay between the two arms is increased and in this time slot it can be seen to have a large phase deviation from the theoretical correlation trace.

The time scale for the plots in Figures 4.10-4.13 is still too large to accurately visualize the phase errors of the traces. Although the trace in Figure 4.12 looks to match the theoretical trace perfectly, a more accurate representation reveals otherwise.

To accurately calculate the phase deviation of the experimental trace, the zero crossings were found and compared to the theoretical zero crossings. Theoretical zero crossings were obtained from the inverse Fourier transform of the measured spectrum shown in Figures 4.8 and 4.9 for Experiments A and B respectively.

The differences between the experimental and theoretical zero crossings gives the phase errors of the experimental traces and are shown in Figures 4.14 for Experiment A

and Figure 4.15 for Experiment B. The data is plotted phase error versus peak number and the peak number 784 corresponds to the zero crossing just to the right of the center of the interferograms. The upper plots show the phase error is much smaller near the center of the interference pattern than at the edges.

The lower plots in the figures show the same phase error data as the upper plots but on a smaller time scale in order to see the phase variation for the center fringes.

The standard deviation was calculated for the data by calculating the mean of the phase errors and subtracting this from each data point. These values were then squared and summed up. The standard deviation was then the square root of this summation divided by the number of samples[22].

$$STD = \left[\frac{1}{N} \sum_{i=1}^{N} (X_i - \mu)^2 \right]^{\frac{1}{2}} \tag{4.2}$$

where N is the number of samples, X_i is the data points, and μ is the mean.

Only data near the center of the fringe pattern was used to calculate the standard deviations. For Experiment A (Figure 4.14) and using the center 100 points of the data from zero crossing 674 to 884, the standard deviation was found to be $3.444 \bullet 10^{-16}$ seconds. For the same sample window in Figure 4.15, the standard deviation was found to be $3.875 \bullet 10^{-16}$ seconds.

A larger sample window of 400 points from 600 to 1000 was used next and the standard deviation for Experiment A was $3.245 \bullet 10^{-16}$ seconds and $5.691 \bullet 10^{-16}$ seconds for Experiment B.

Clearly the phase errors were larger in Experiment B explaining why the calculated spectrum from this data was more inaccurate than that calculated in Experiment A.

The source of these errors has not been determined but a possible reason could be the step size of the translation stage is not perfectly equal for each step. Another source of error could be the vibration of the mounts holding the mirrors as the stage is moved.

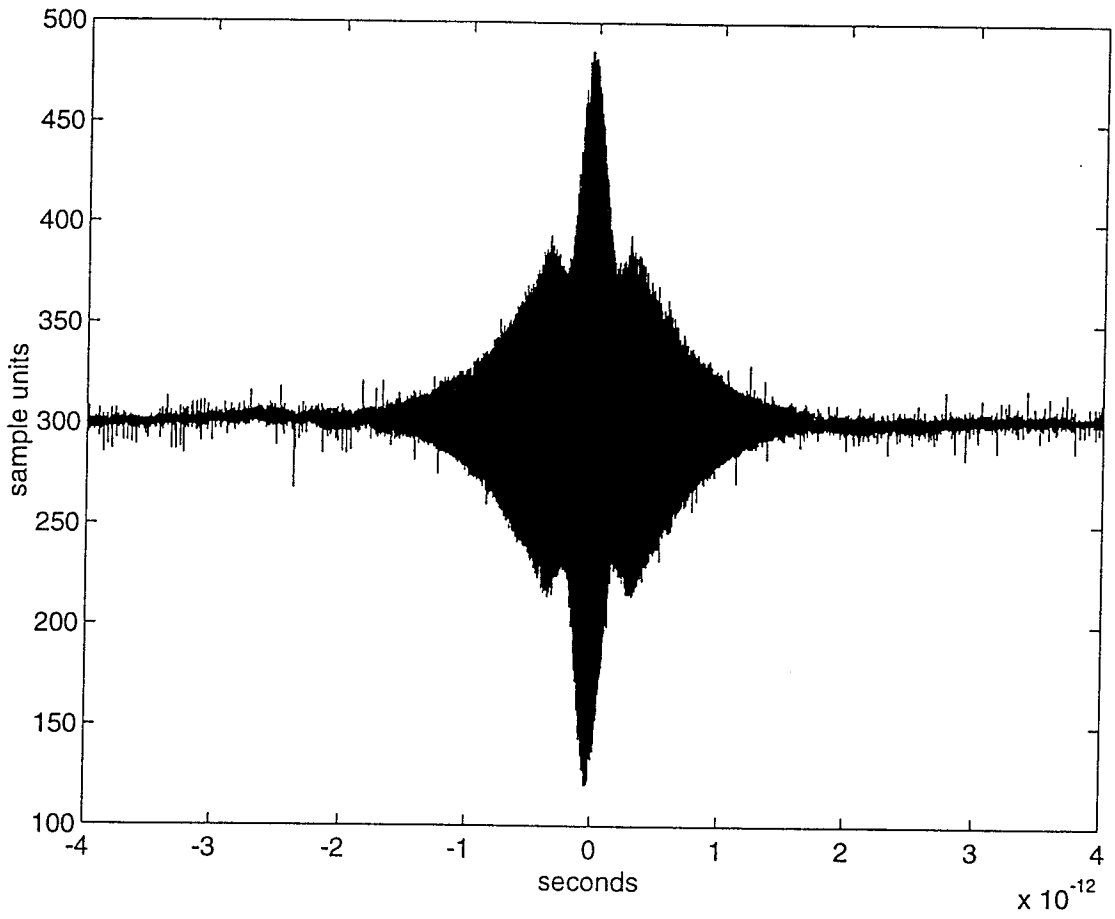

Figure 4.4 8 Picosecond One Pass Scan

Experiment B

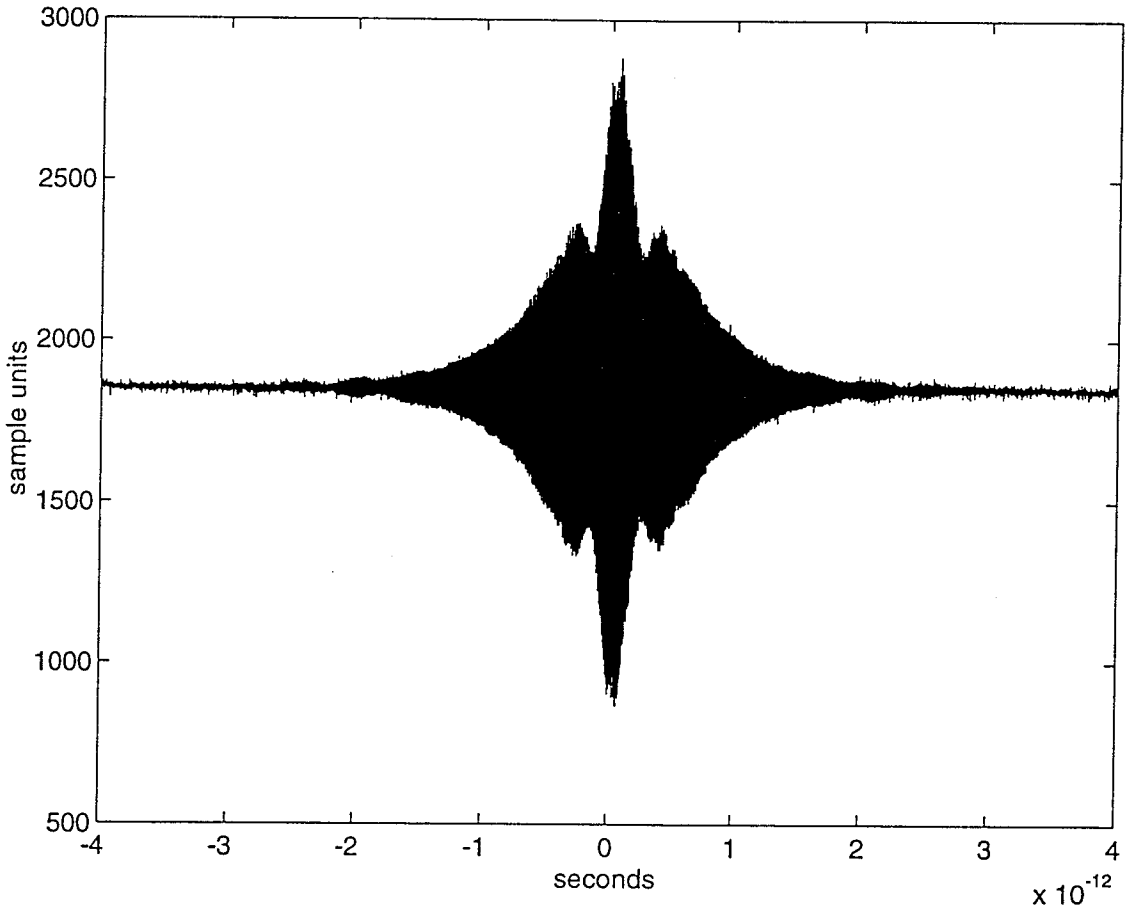

Figure 4.5 .8 Picosecond Six Pass Scan

Experiment B

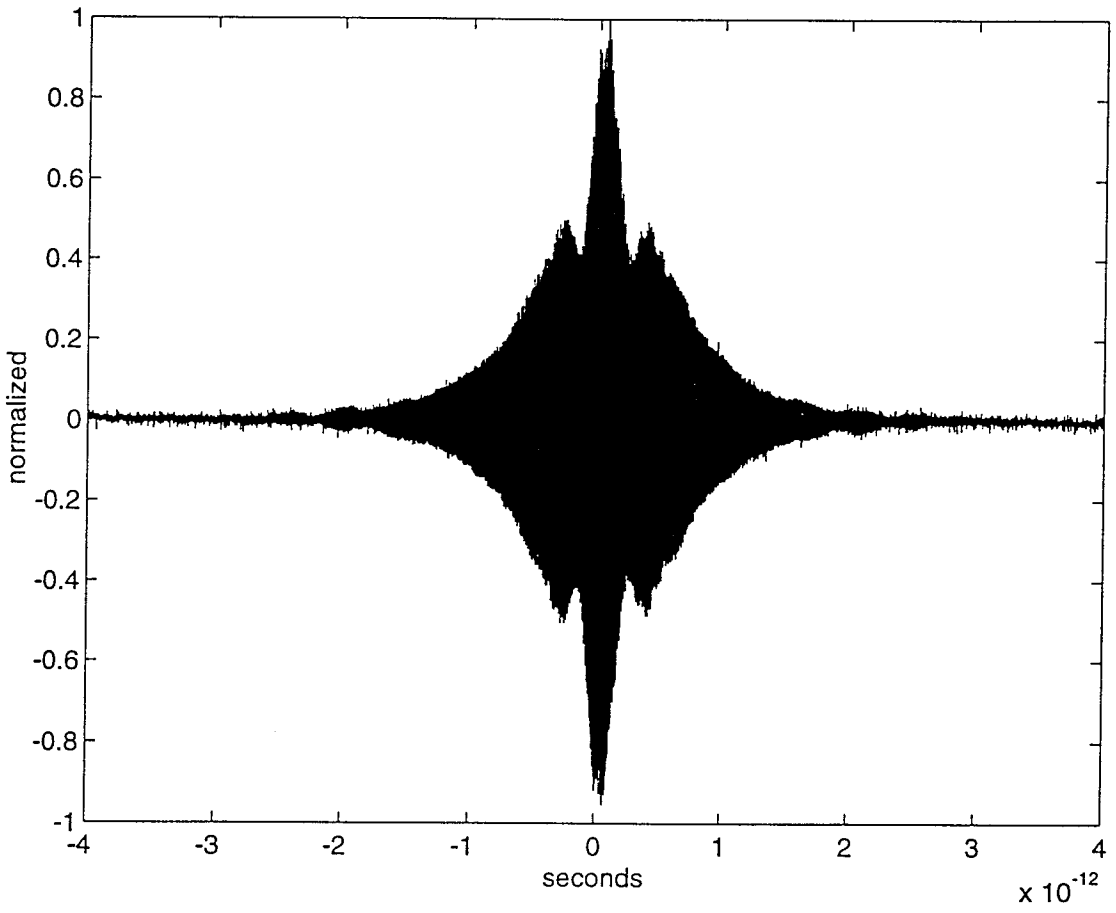

Figure 4.6 8 Picosecond Six Pass Normalized Scan

Experiment B

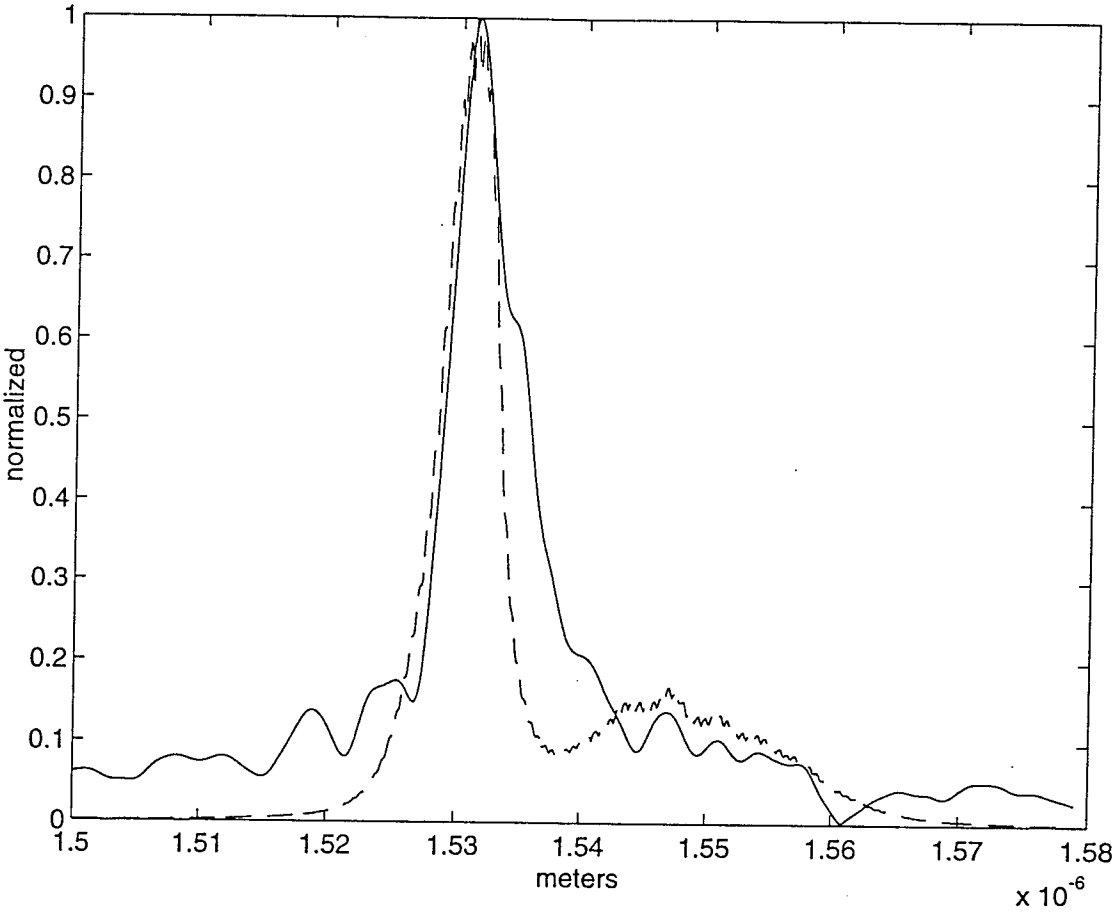

Figure 4.7 Plot of Measured Spectrum(--) and Calculated Spectrum(-)

Experiment B

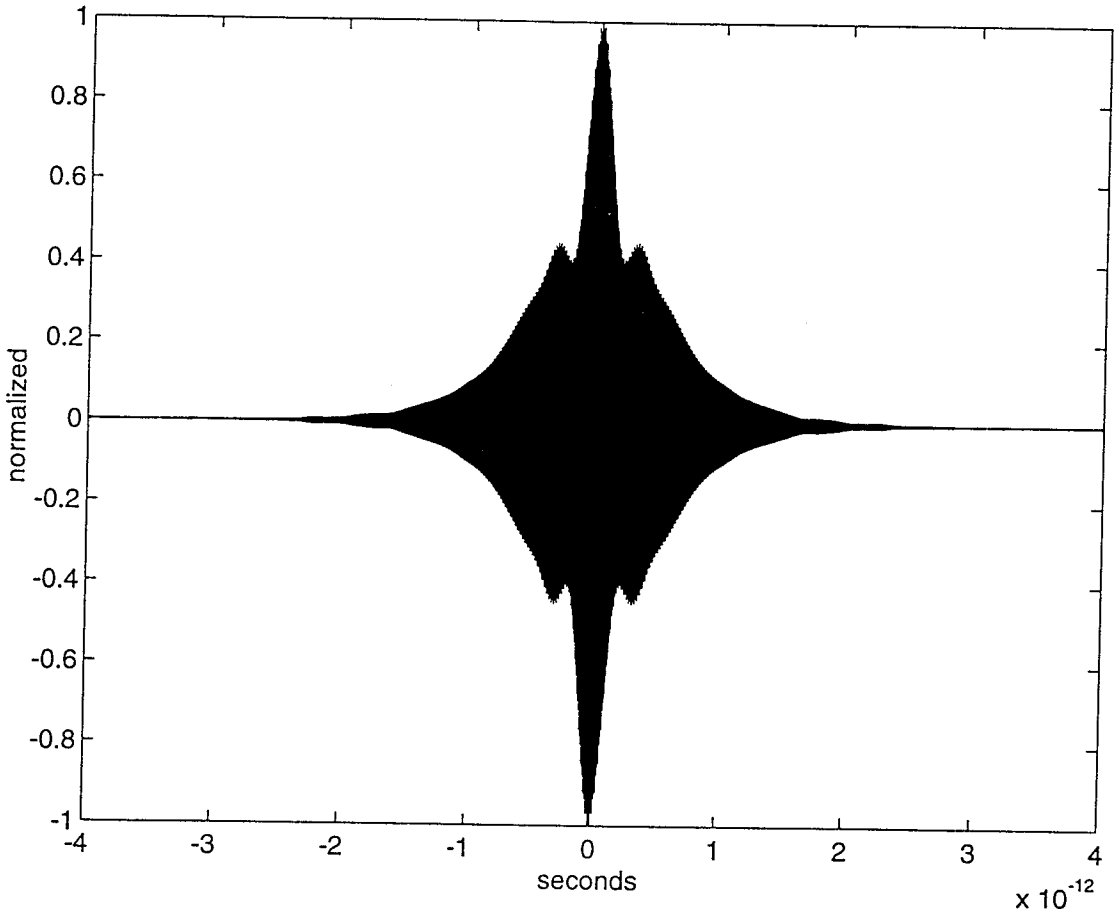

Figure 4.8 Theoretical Electric Field Correlation Calculated from Measured Spectrum Experiment A

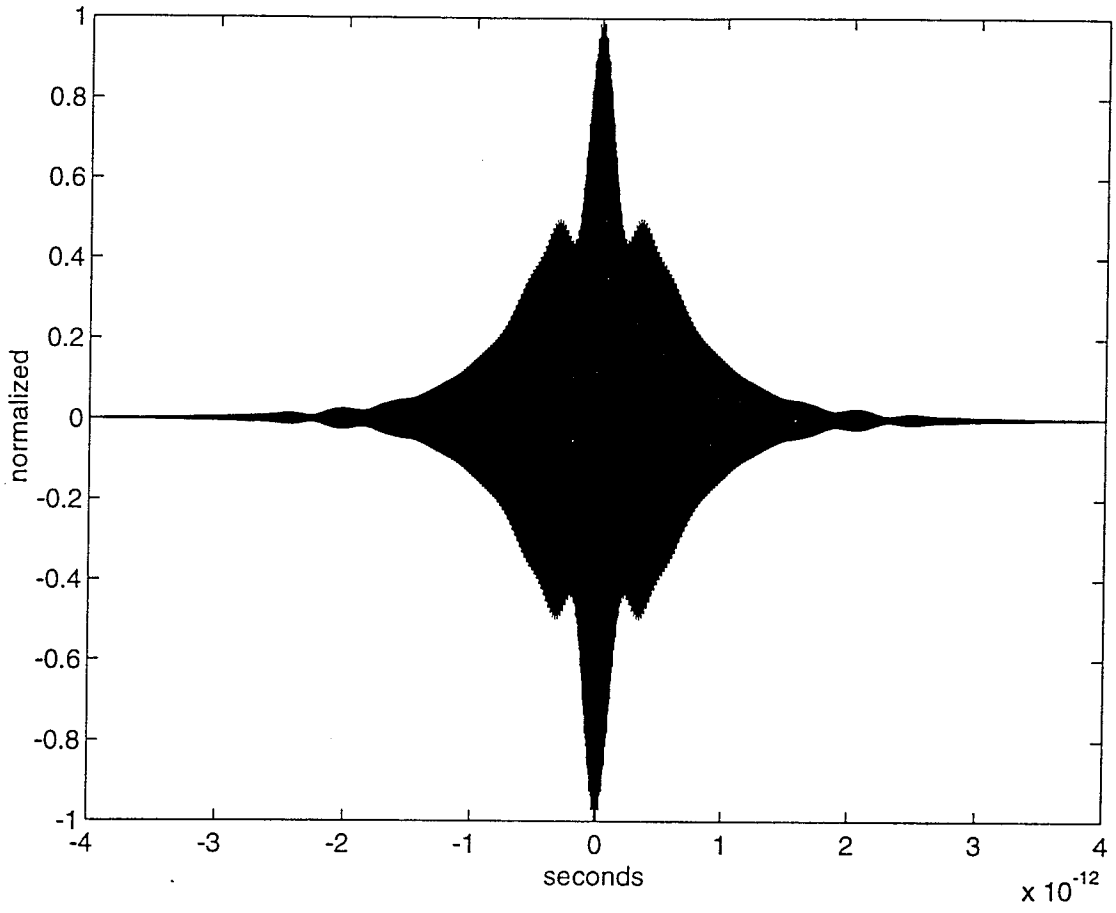

Figure 4.9 Theoretical Electric Field Correlation Calculated from Measured Spectrum Experiment B

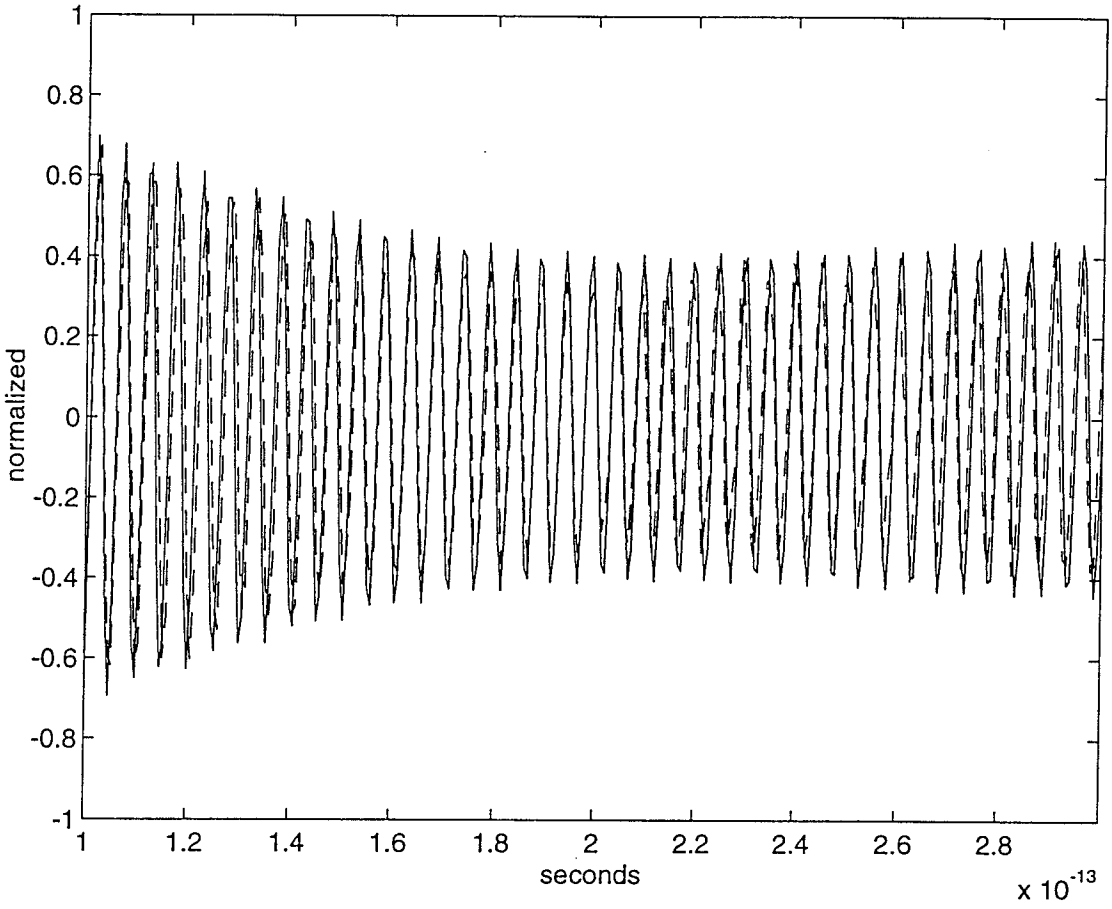

Figure 4.10 Blow Up of Experimental and Theoretical Correlation Fringe Pattern Experiment A

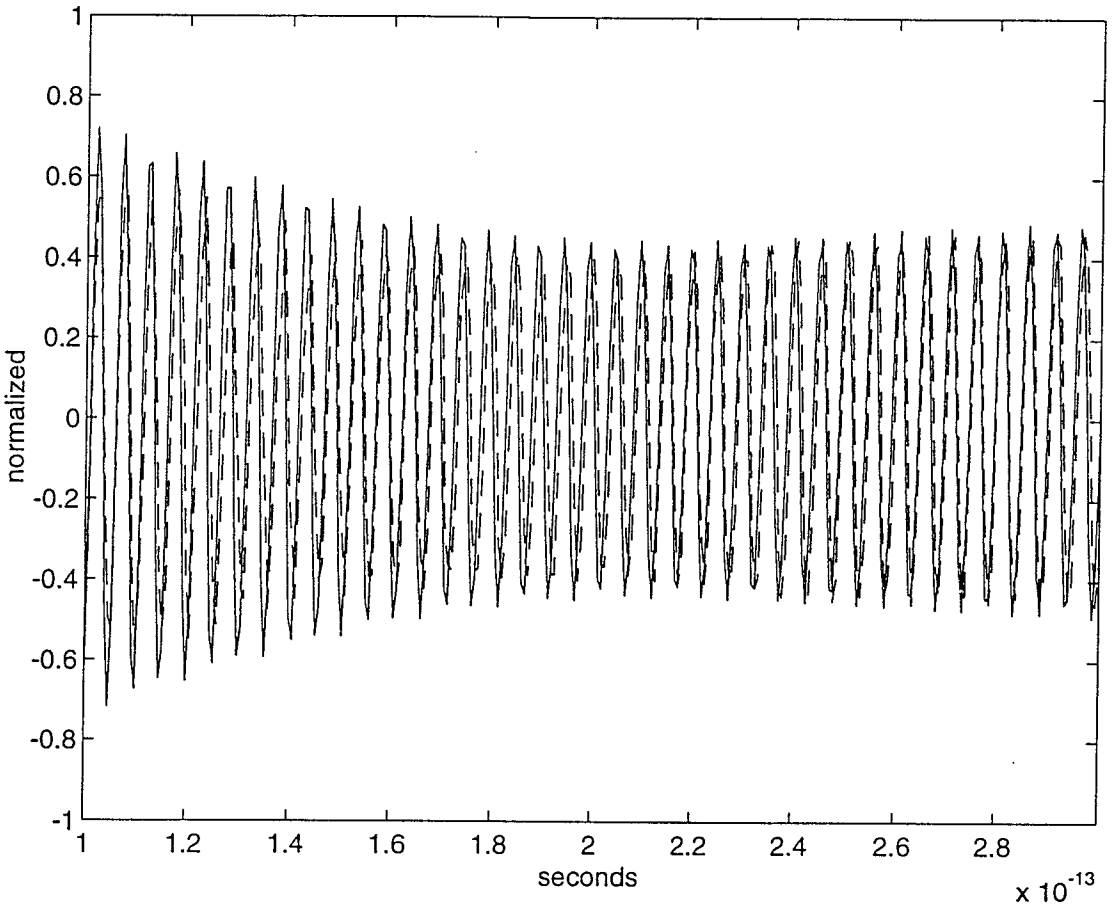

Figure 4.11 Blow Up of Experimental and Theoretical Correlation Fringe Pattern Experiment B

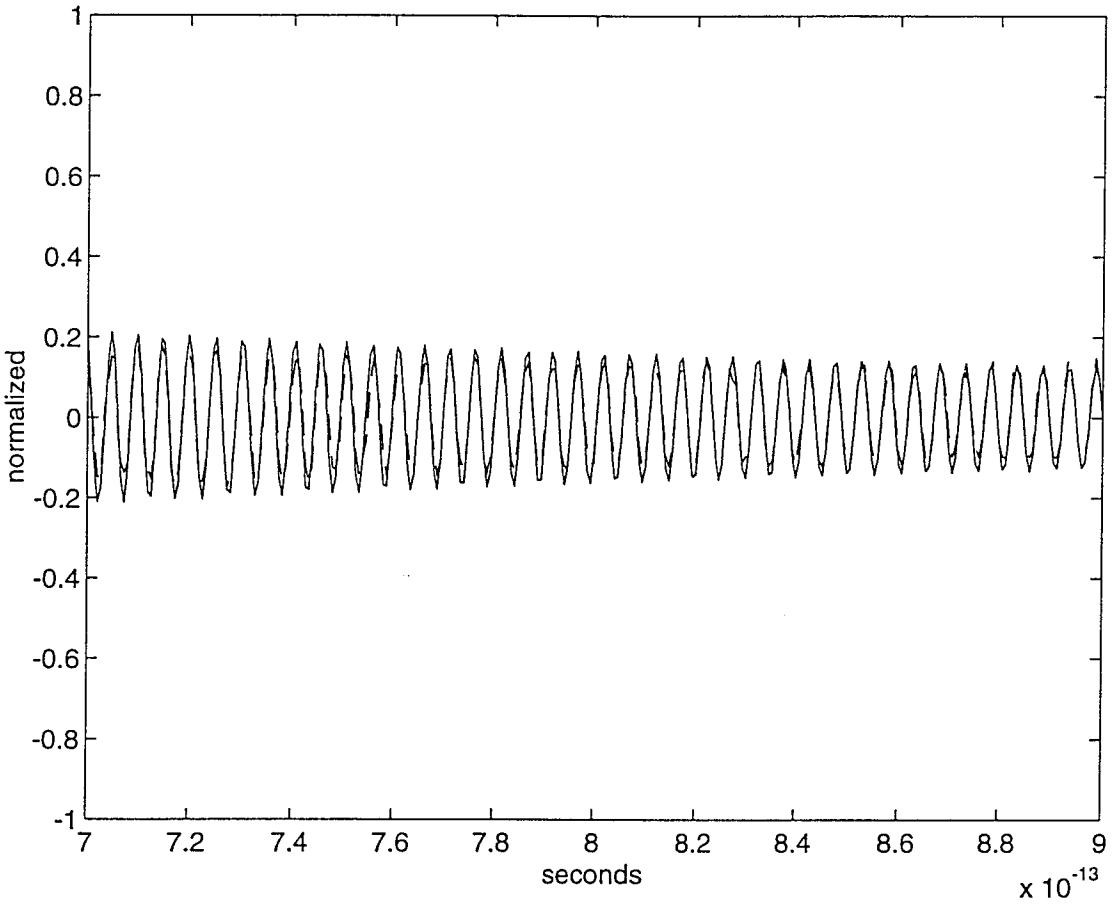

Figure 4.12 Blow Up of Experimental and Theoretical Correlation Fringe Pattern Experiment A

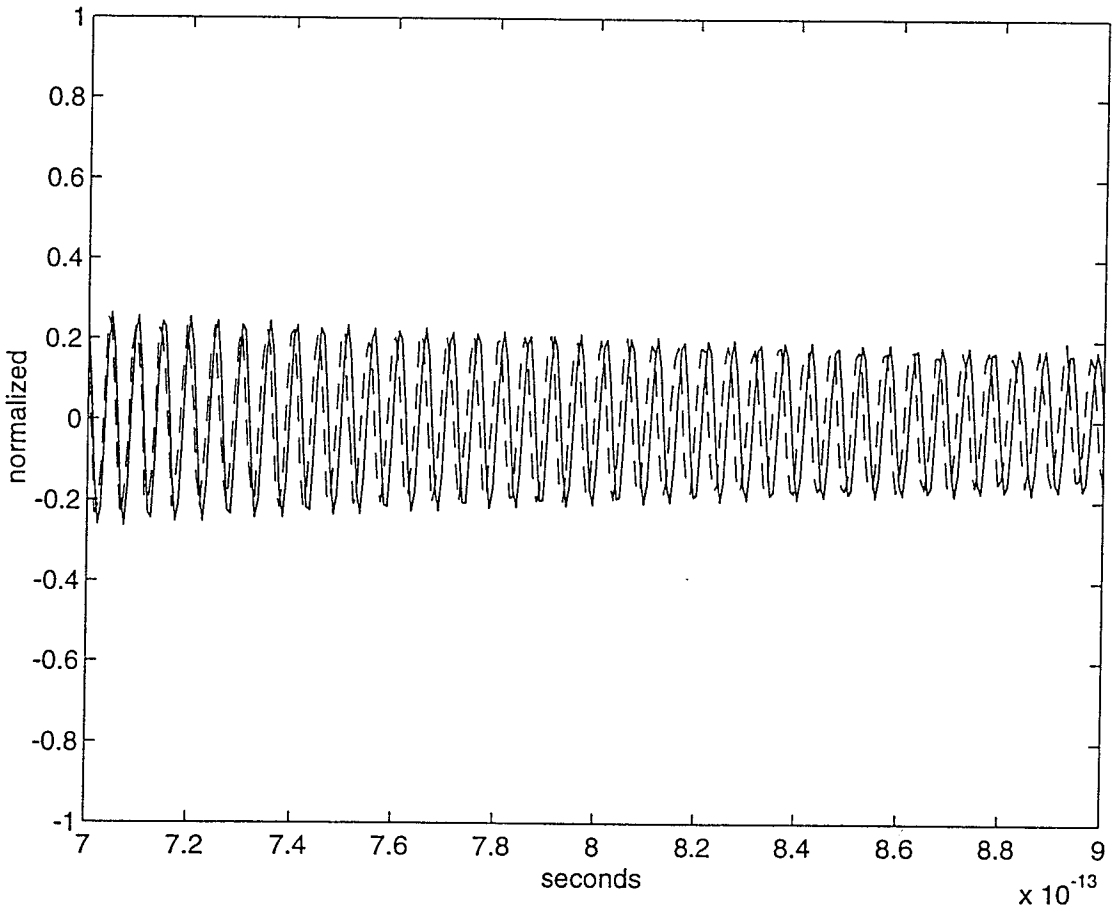

Figure 4.13 Blow Up of Experimental and Theoretical Correlation Fringe Pattern Experiment B

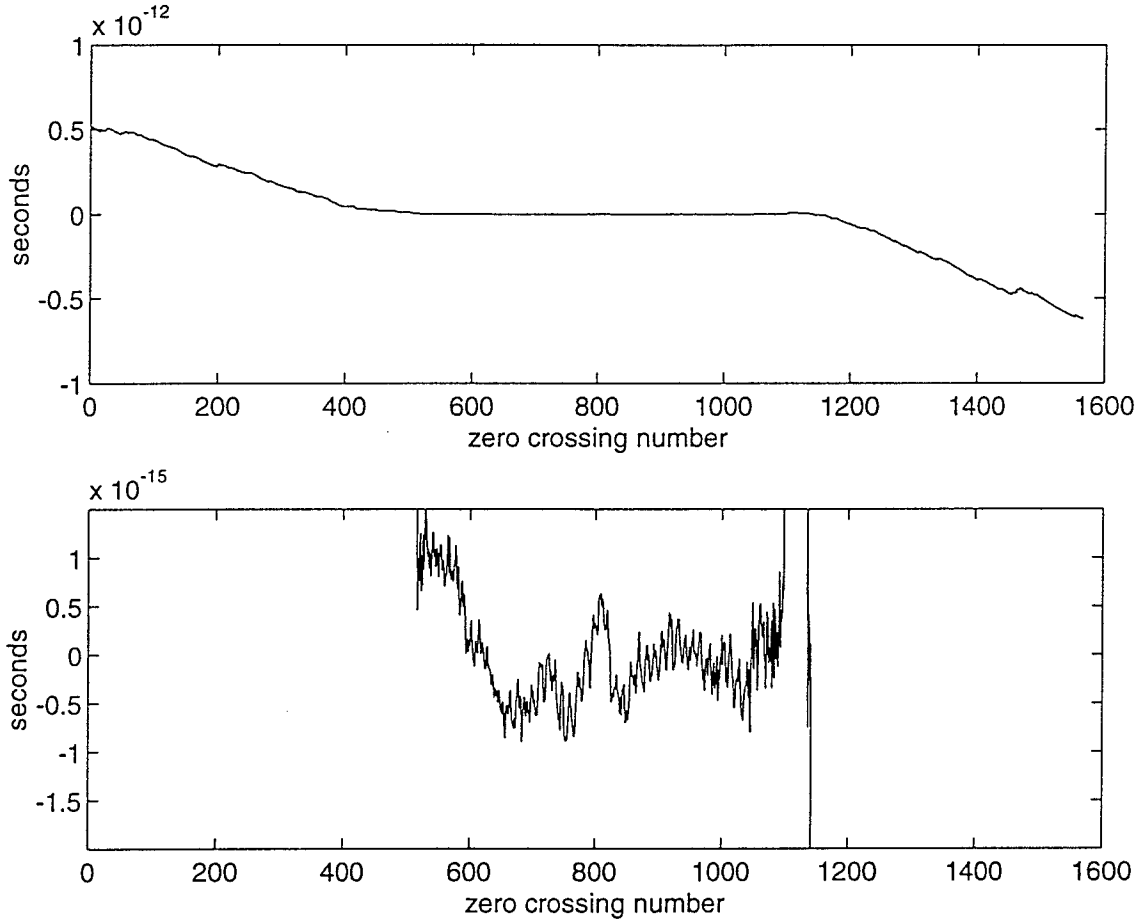

Figure 4.14 Phase Error for Experiment A

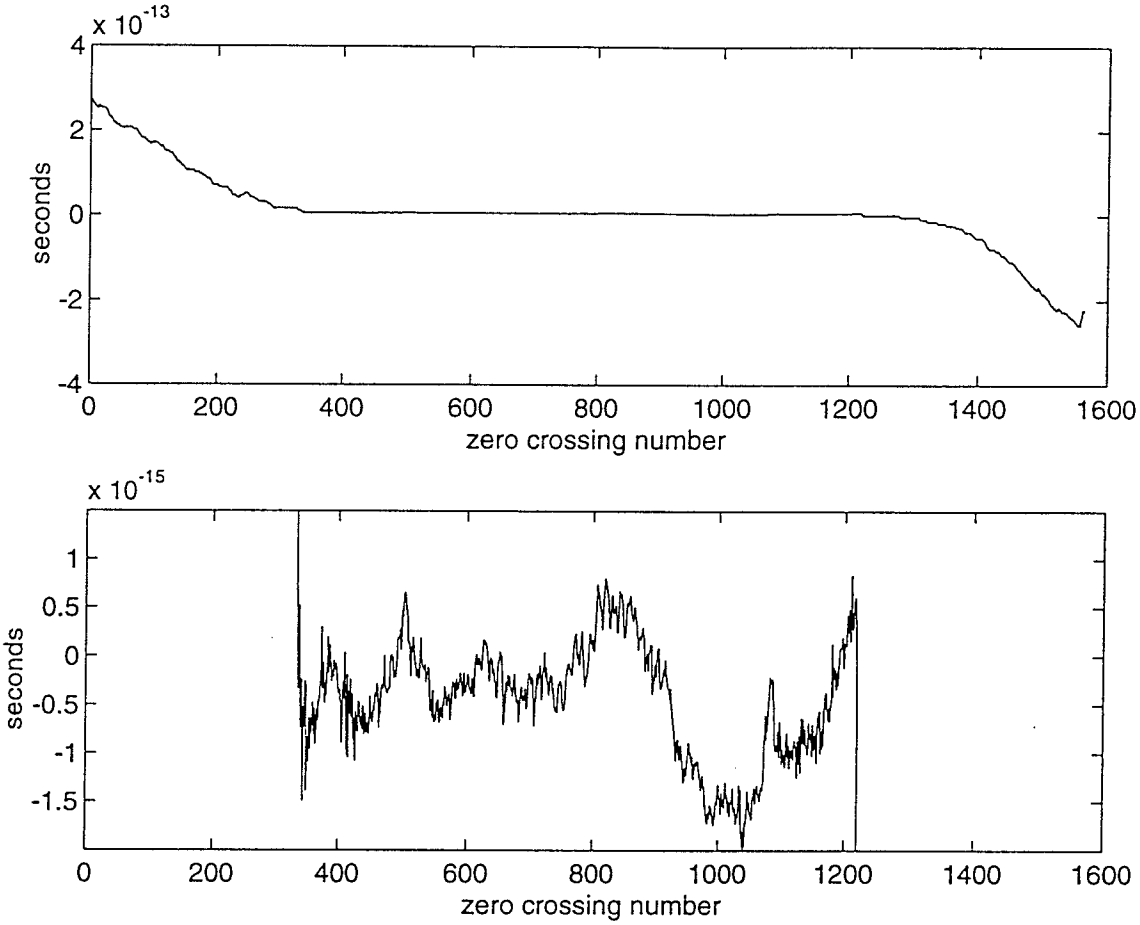

Figure 4.15 Phase Error for Experiment B

4.2. EFFECT OF SILICON FILTER IN SOURCE

A small portion of the ASE passing through the silicon filter in the source is internally reflected in the filter and then passed into the interferometer. This light is delayed behind the first pass light by a time of

$$\delta t = \frac{2d}{c}\left[n - \lambda_o \frac{dn}{d\lambda}\right] \tag{4.3}$$

where the term in the brackets is the group index of refraction of the silicon wafer, d is the thickness, λ_o is the center frequency, 1540 nm, and c is the speed of light. The group index of refraction n_g, takes into account the dispersion of light through the sample due to different velocities of propagation for different wavelengths.

The index of silicon at 1530 nm is 3.4794, at 1540 is 3.4785, and at 1550 nm is 3.4777[23]. From this, the group index is found to be n_g=3.6094.

The thickness of the silicon wafer was measured with a micrometer and found to be 22.5 mils(0.572 mm). Using equation 4.3, the center of the fringe pattern replicas should be at positive and negative 13.7 ps. Due to the limited scan range of the data acquisition memory, the replicas and the main interferogram could not be captured in the same scan. Manually moving the stage and monitoring the photodiode output on an oscilloscope, the center of the fringe patterns were found to be at the expected time delay of 13.7 ps.

Removing the wafer did not effect the position of the main interferogram located at zero delay. It did, however, remove the replicas of the fringe pattern that were seen before because the Fabry Perot cavity was gone. The position of the main fringe pattern did not shift even though the light was delayed through the filter because both arms experienced the phase shift. A shift in the pattern would result when only one arm experiences a phaseshift.

With the wafer in place, fringe patterns theoretically should have been seen at all multiples of δt, and not just 13.7 ps (first order replica). The amplitudes of the higher order replicas were so small, any trace of them was lost in noise and could not be detected. The amplitudes of the first order replicas were rather small as it was. These

replicas were not recorded so the actual amplitudes could not be determined. Theoretical amplitudes of the replicas can be found from the reflection coefficient determined by the indices of refraction[18] for silicon(n_g=3.6094) and air(n_a=1).

$$\rho = \frac{n_g - n_a}{n_g + n_a} \tag{4.4}$$

This results in a coefficient of 0.545 and the delayed field amplitude then would be 30% of the first field through. The second order replicas would theoretically have amplitudes of 8% of the first field through and probably undetectable through the noise.

The higher order replicas did not have enough power to be detected once they traveled through the interferometer.

5. MEASUREMENTS OF SAMPLES IN INTERFEROMETER

5.1 INTRODUCTION

When a sample was placed in one arm of the interferometer, the fringe patterns shifted due to a change in the optical path length through the sample. The amount of change varied greatly depending on the sample used. Three different samples were used and the effects they had on the fringe pattern are discussed. The samples were a 1 mm thick microscope slide, a 100 μm thick microscope slide, and a 0.5 mm thick silicon wafer similar to the one used as the 980 nm filter in the source. Figure 5.1 shows an interferometric scan for each of the four conditions: no sample, 100 μm slide in one arm, 1 mm slide in one arm, and the silicon wafer in one arm. In all the scans, the dc component was removed by subtracting off the mean, and then the amplitudes were normalized with respect to the peak power of the scan. The zero delay position was kept constant for all scans in order to see the effect the sample had on the fringe pattern. The blank scan case has been discussed previously and is used to compare the other three cases below.

5.2 1 mm THICK MICROSCOPE SLIDE

A glass microscope slide with a measured thickness of 0.99 mm was placed in the sample arm of the interferometer. The light propagated through the sample with a group velocity:

$$v_g = \frac{c}{n - \lambda_o \frac{dn}{d\lambda}} \tag{5.1}$$

The time difference between light propagating in the sample arm and light in the reference arm was:

$$\delta t = \frac{d}{c}[n - \lambda_o \frac{dn}{d\lambda} - 1] \tag{5.2}$$

Glass has a group index of about 1.5 which leads to a theoretical delay of 1.65 ps for this slide and the center of the fringe pattern was found at this delay time.

It can be seen from Figure 5.1 that the presence of this sample did not alter the shape or size of the inteferogram any noticeable amount.

From equation 4.3 replicas of the inteferogram should have been seen at multiples of 9.9 ps from the center of the main fringe pattern. These fringes should occur only at positive multiples of this time[8], because the light reflecting in the slide caused a positive delay. The fringes were unable to be detected in the presence of the noise due to their minimal amplitude. From equation 4.4, the field amplitude of the first order reflected wave is 4% of the original field using n_g=1.5. Due to this fact, these fringes were not detectable in the presence of noise. The only fringe patterns seen were the interference patterns discussed in section 4.2 from the silicon wafer in the source which were displaced by 13.7 ps either side of the shifted main interferogram.

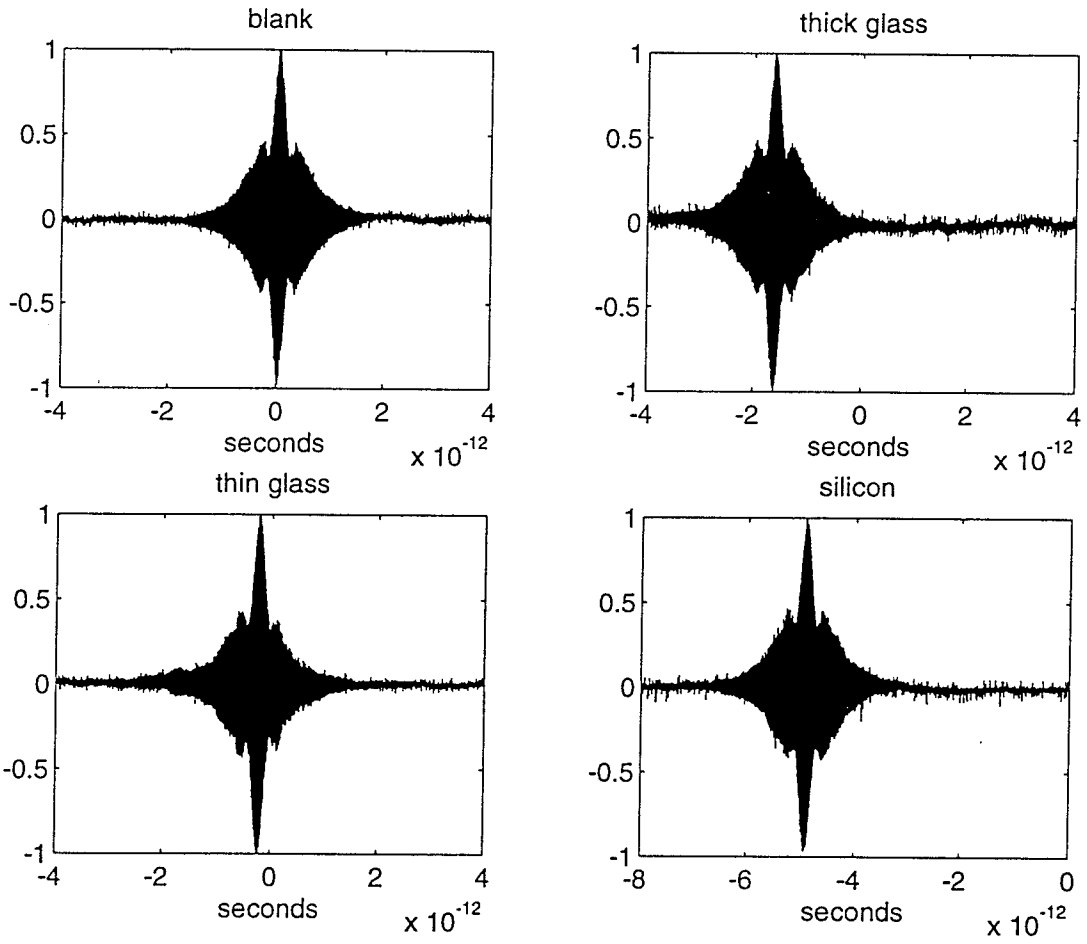

Figure 5.1 Correlation Scans With Different Samples Present

5.3 100 μm THICK MICROSCOPE SLIDE

The next sample placed in the interferometer was another glass microscope slide, this time the measured thickness was 152.4 μm. Similar analysis to that of the thick slide gives a theoretical shift of the interference fringes of 0.25 ps which was the value found experimentally and seen in Figure 5.1.

Also seen in Figure 5.1 is the presence of an extra hump in the scan data located about 1.5 ps to the right of the center of the main lobe. From equation 4.3, the cavity delay time for the glass slide was found to be this value.

The thin glass slide and thick glass slide both had the same index of refraction and therefore the same reflection coefficient and the same amount of power in the first replica, 4%. A reason the replica could be detected with the thin glass slide was because the round trip cavity time was still within the interference time of the first through light, about 1.5 ps either side of zero delay. Thus, the delayed light interacted with the stronger undelayed light and the fringes could be seen. In the thick slide, the delay time was much longer than the interference time of the first light and therefore no interaction took place and was not detected above the noise.

5.4 SILICON WAFER

The last sample used was a silicon wafer similar to the one used in the source. This sample should theoretically produce a delayed first order with 30% of the original power which should be large enough to overcome the noise and be detected.

As shown in Figure 5.1, the main fringe pattern was delayed by 4.95 ps which matches the theoretical delay calculated from equation 5.2.

The silicon wafer in the source was removed and the delay was scanned centered around 13.7 ps either side of the shifted main lobe. This time, the interference fringes due to the sample only were detected. The interference pattern was seen only on the positive delay side of the main lobe as seen in the thin glass slide experiment and expected[8].

When the silicon wafer was replaced in the source, the fringe pattern was again detected at negative multiples of the delay time as well. A difference is noted in using

this sample as compared to the previous two. In the previous examples using glass, the delay periods of the sample did not overlap those of the wafer in the source. If there was any overlap, the effect was minimal and not noticeable due to the minimal power carried by the reflected light from the sample.

With a sample consisting of a similar wafer to that in the source, the delay periods matched up with each other and fringe replicas had significant amplitudes. The effect of this was the fringe patterns with positive delays having larger amplitudes than the patterns experiencing negative delays. This is easy to explain if the light is thought of as a pulse.

When the light pulse goes through a silicon wafer, part of it is internally reflected and then transmitted later at a time equal to the cavity round trip time given in equation 4.3. As shown in section 4.2, the first echoed pulse will have a field amplitude about 30% of the original. There will be more pulses at integer multiples of the delay time, but the energy of these pulses is insignificant and will be ignored in this analysis. Figure 5.2 is a graphical representation of these pulses. The original pulse is assumed to have an energy of 1 unit, therefore the delayed pulse will have an amplitude of 0.3 units. The pulse spacing is set to the cavity delay time and the x axis is time.

Figure 5.3 shows what happens to the pulse train when it is delayed by a delay τ. Scanning the translation stage in the reference arm, has the effect of adjusting the delay from values of negative τ to positive τ. This causes the fields from the two arms to be correlated. The result of correlating Figure 5.2 and Figure 5.3 is shown in Figure 5.4 as a function of the delay, τ. As expected, the largest amplitude is at a delay of zero corresponding to when all the pulses match up perfectly.

Figure 5.4 represents the fringe pattern when a silicon wafer is present only in the source. When a silicon wafer is placed in the sample arm, the light traveling through this arm alone is correlated twice and can be represented by Figure 5.4 also. Now, at the output of the interferometer, this light is correlated with the light from the reference arm represented by Figure 5.3.

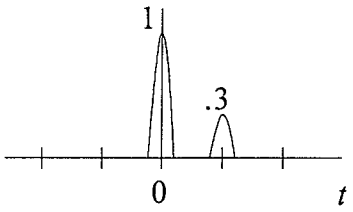

Figure 5.2 Pulse Representation of Light Through Sample

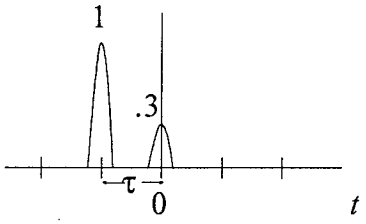

Figure 5.3 Light Pulses With Delay

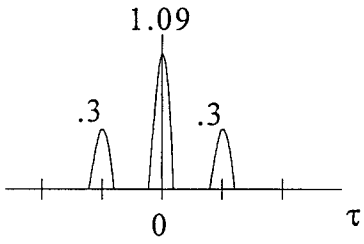

Figure 5.4 Correlation of Delayed and Undelayed Light Pulses

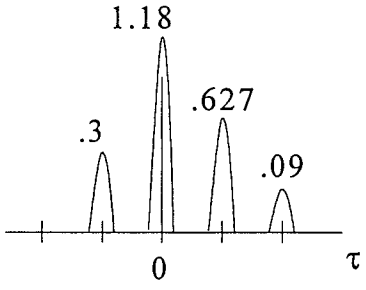

Figure 5.5 Result of Correlation of Figure 5.3 and Figure 5.4

Correlating the pulses from both arms produces the pulse train as depicted in Figure 5.5. The pulses to the right of zero delay(positive delay) are larger than those to the left of the main pulse(negative delay) which agrees with the experimental results.

The scan time available was not enough to capture the main interferogram and these replicas in one scan.

Figure 5.6 is the main interferogram centered at zero delay. This scan data was acquired over 5 scans. The first replica with a positive delay is shown in Figure 5.7 which was acquired over 7 scans. Finally, the replica at a delay of -13.7 ps is shown in Figure 5.8. This scan was acquired over 10 passes. To accurately compare these three fringe patterns to determine if the amplitudes match the predicted values in Figure 5.5, the amplitudes of the interferograms have to be divided by the number of scans they were acquired over. Doing so, the positive delayed satellite had an amplitude that was 35% of the original fringe pattern. The amplitude of the replica on the other side was 15% of the original. These numbers are about half the predicted size. A reason the amplitudes were not as high as predicted could be because the light from the two arms of the interferometer were not perfectly aligned and the beams walked off from each other as the stage was scanned. Another possibility could be the thickness of the two wafers were not exactly the same which would cause phase differences between the delayed fields and original field. The result would be the light not constructively interfering 100% and the values shown in Figure 5.5 being larger than experimentally measured.

Figure 5.9 is a composite of these three interferograms. Each scan was divided by the number of passes taken to acquire the data in order to determine the amplitude of a single scan. The three scans were then normalized to the peak power of the largest. The x axis is time and the y axis is normalized units.

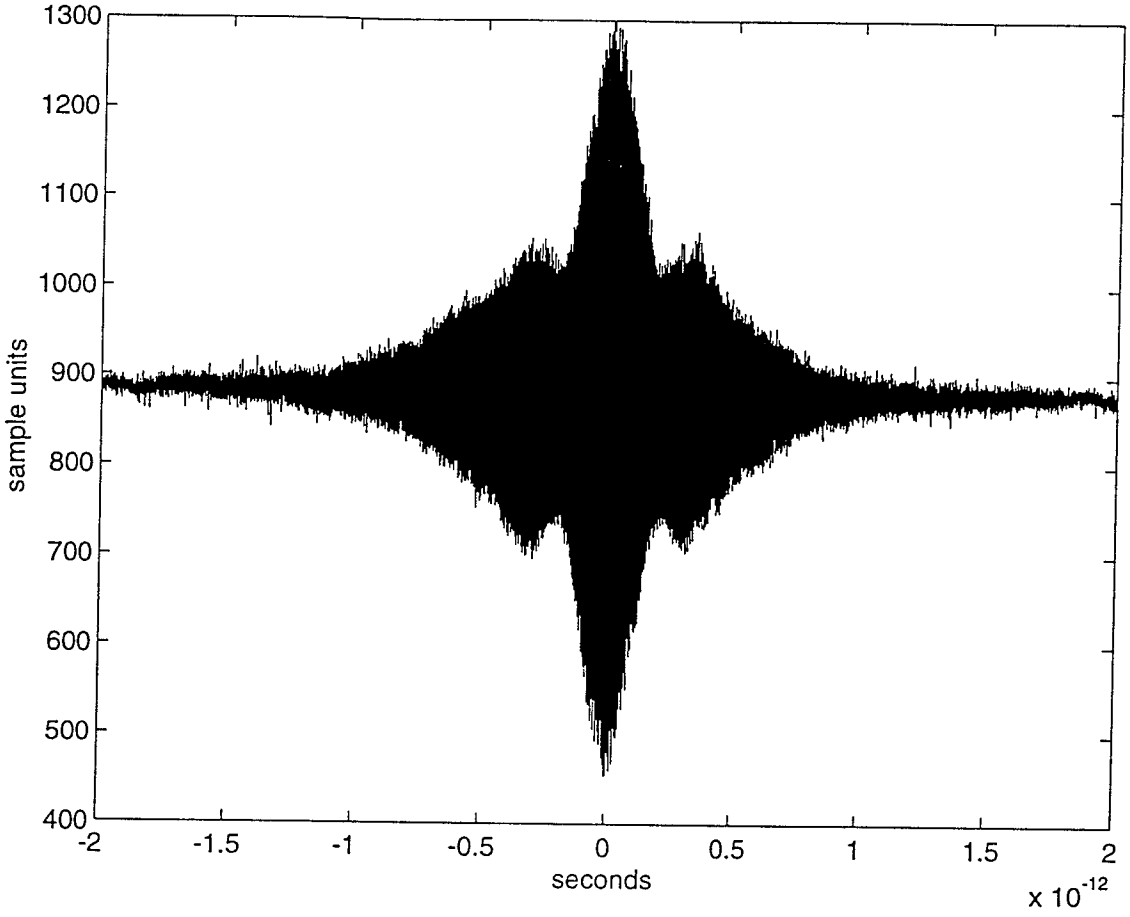

Figure 5.6 4 Picosecond Scan of Interferogram at Zero Delay

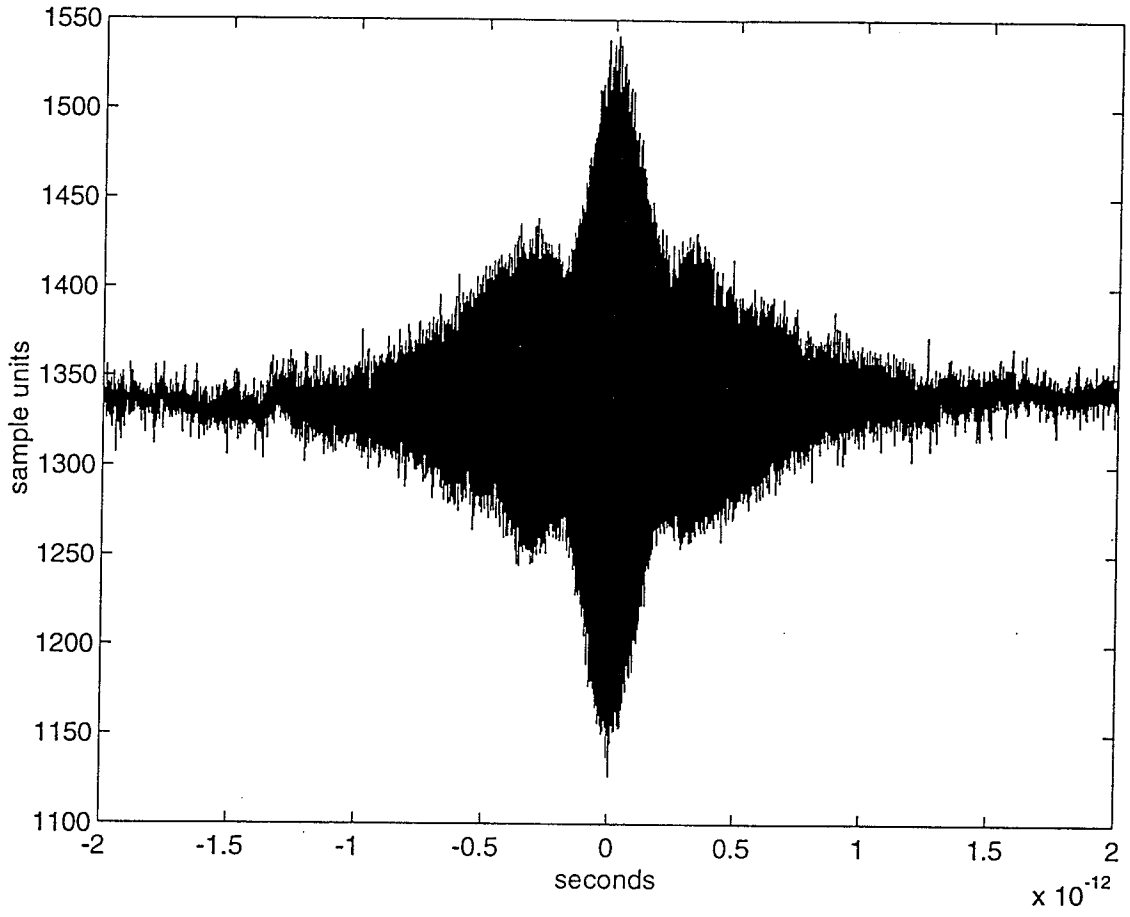

Figure 5.7 Interference Fringes of Delayed Replica Centered at +13.7 ps.

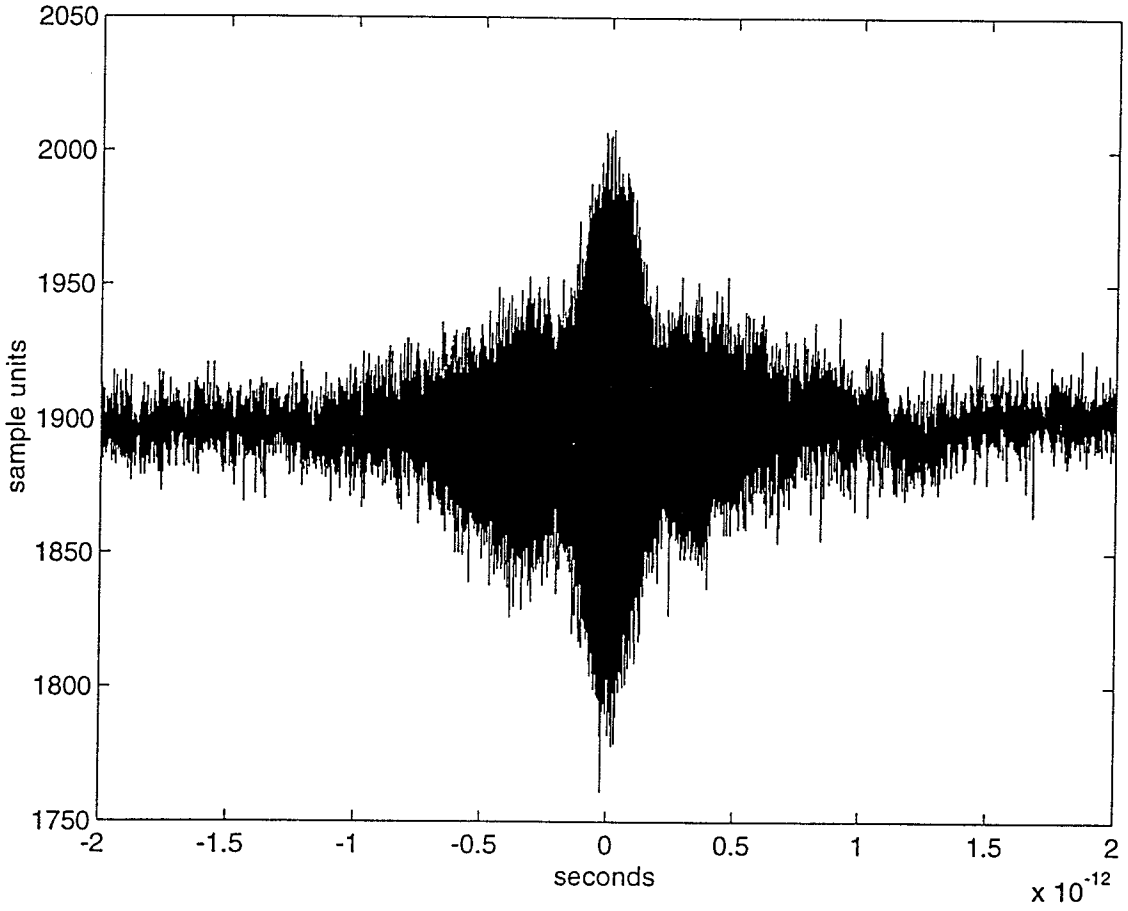

Figure 5.8 Interference Fringes of Delayed Replica Centered at -13.7 ps.

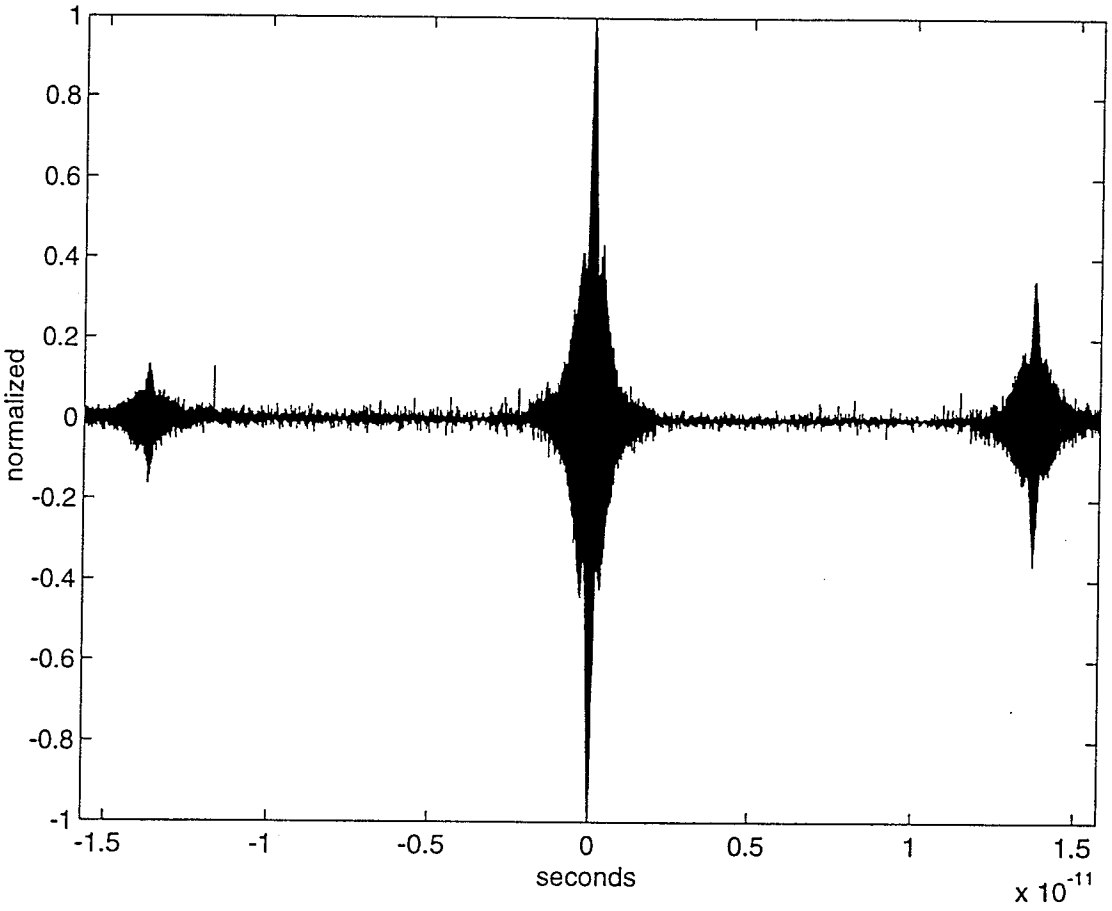

Figure 5.9 Normalized Composite of Main Correlation Fringes and its Satellites

6. CONCLUSION

A Ti:sapphire pumped Erbium doped fiber proved to be a good source for wide band white light around 1540 nm. The few milliwatts of output power was sufficient to enable interferometric data to be taken.

Using a Mach Zehnder interferometer with a variable path length in one arm, the correlation of the two arms could be recorded. Accuracy of the correlation fringes was tested by Fourier transforming the fringe pattern and comparing the resulting spectrum to the measured spectrum. The spectra calculated from the intererence patterns were full of inaccuracies due to phase errors in the scan data. These phase errors could be the result of vibrations in the experimental setup or unequal step size due to an inaccuracy in the translation stage.

Placing a sample in on arm of the interferometer had the effect of delaying the light through that arm by an amount equal to the round trip cavity time. If the sample was more dispersive or altered the spectrum of the light as it passed through, the correlation shape would be altered.

An alternative to putting a sample material in the interferometer to change the spectral components of the light is to put a pulse shaper into the sample arm[25,26]. By changing the spectral shape of the source light using a mask, the shape of the correlation can be drastically changed. This is the basis of future work in the experimental setup.

LIST OF REFERENCES

[1] R. L. Fork, C. H. Brito, P. C. Becker, and C. V. Shank, "Compression of optical pulses to six femtoseconds by using a cubic phase compensation," *Optics Letters*, vol. 12, pp. 483-485, July 1987.

[2] W. H. Knox, R. L. Fork, M. C. Downer, R. H. Stolen, and C. V. Shank, "Optical Pulse Compression to 8 fs at a 5 -kHz Repetition Rate," *Applied Physics Letters*, vol. 46, pp. 1120-1121, June 1985.

[3] W. H. Knox, N. M. Pearson, K. D. Li, and C. A. Hirlimann, "Interferometric Measurements of Femtosecond Group Delay in Optical Components," *Optics Letters*, vol. 13, pp. 574-576, July 1988.

[4] M. Beck, I. A. Walmsley, and J. D. Kafka, "Group Delay Measurements of Optical Components Near 800 nm," *IEEE Journal of Quantum Electronics*, vol. 27, pp. 2074-2081, August 1991.

[5] M. Beck and I. A. Walmsley, "Measurment of Group Delay With High Temporal and Spectral Resolution," *Optics Letters*, vol. 15, pp. 492-494, May 1990.

[6] K. Naganuma, "Semiconductor Laser Cavity Dispersion Measurement Based on Interferometric Crosscorrelation of Amplified Spontaneous Emission," *Applied Physics Letters*, vol. 64, pp. 261-263, January 1994.

[7] K. Naganuma and Y. Sakai, "Interferometric Measurement of Wavelength Dispersion on Femtosecond Laser Cavities," *Optics Letters*, vol.19, pp. 487-489, April 1994.

[8] K. Naganuma and H. Yasaka, "Group Delay and a-Parameter Measurement of 1.3 mm Semiconductor Traveling-Wave Optical Amplifier Using the Interferometric Method," *IEEE Journal of Quantum Electronics*, vol. 27, pp. 1280-1287, June 1991.

[9] H. Haus, *Waves and Fields in Optoelectronics*. Englewood Cliffs, NJ: Prentice-Hall, Inc. 1984.

[10] E. Hecht, *Optics*. Reading, Mass: Addison-Wesley Publishing Company, 1987.

[11] E. Desurvire and J. Simpson, "Amplification of Spontaneous Emission in Erbium Doped Single-Mode Fibers," *Journal of Lightwave Technology*, vol. 7, pp. 835-845, May 1989.

[12] P. F. Wysocki, M. J. F. Digonnet, B. Y. Kim, and H. J. Shaw, "Characteristics of Erbium-Doped Superfluorescent Fiber Sources for Interferometric Sensor Applications," *Journal of Lightwave Technology*, vol. 12, pp. 550-567, March 1994.

[13] C. R. Giles and E. Desurvire, "Modeling Erbium-Doped Fiber Amplifiers," Journal of Lightwave Technology, vol. 9, pp. 271-282, February 1991.

[14] E. Desurvire, M. Zirngibl, H. M. Presby, and D. DiGiovanni, "Characterization and Modeling of Amplified Spontaneous Emission in Unsaturated Erbium-Doped Fiber Amplifiers," *IEEE Photonics Technology Letters*, vol. 3, pp. 127-2081, February 1991.

[15] Personal communication with Dan Leaird

[16] S. M. Sze, *Physics of Semiconductor Devices*. New York, NY: John Wiley & Sons, 1981.

[17] A. Oppenheim, A. Willsky, and I. Young, *Signals and Systems*. Englewood Cliffs, NJ: Prentice-Hall, Inc. 1983.

[18] S. Ramo, J. Whinnery, and T. Van Duzer, *Fields and Waves in Communication Electronics*. New York, NY: John Wiley & Sons, 1984.

[19] K. Naganuma, K. Mogi, and H. Yamada, "Group Delay Measurement Using the Fourier Transform of an Interferometric Cross Correlation Generated by White Light," *Optics Letters*, vol. 15, pp. 393-395, April 1990.

[20] I. N. Duling, R. P. Moeller, W. K. Burns, C. A. Villarruel, L. Goldberg, E. Snitzer, and H. Po, "Output Characeristics of Diode Pumped Fiber ASE Sources," *IEEE Journal of Quantum Electronics*, vol. 27, pp. 995-1003, April 1991.

[21] R. Louden, *The Quantum Theory of Light*, 2nd ed. New York: Oxford Science Publications, 1985.

[22] D. L. Harnett, *Statistical Methods*, 3rd ed. Menlo Park, CA: Addison-Wesley Publishing Company, 1982.

[23] J. F. Shackelford, *CRC Materials Science and Engineering Handbook.* Ann Arbor, MI: CRC Press, 994.

[24] M. A. Saifi, M. J. Andrejco, W. I. Way, A. Von Lehman, A. Y. Yan, Chinlon Lin, F. Bilodeau, and K. O. Hill, "Er3+ -Doped GeO2-CaO-Al2O3 Silica Core Fiber Amplifier Pumped at 813 nm," presented at Optical Fiber Conference, 1991.

[25] A. M. Weiner, J. P. Heritage, and E. M. Kirschner, "High-Resolution Femtosecond Pulse Shaping," *Journal of the Optical Society of America B*, vol. 5, pp. 1563-1572, August 1988.

[26] A. M. Weiner, D. E. Leaird, G. P. Wiederrecht, K. A. Nelson, "Femtosecond Pulse Sequences Used for Optical Manipulation of Molecular Motion," *Science*, vol. 247, pp. 1317-1319, March 1990.